AGU PUBLICATIONS

JGR

Journal of Geophysical Research: Oceans

RESEARCH ARTICLE

10.1002/2016JC012479

# Reverse Estuarine Circulation Due to Local and Remote Wind Forcing, Enhanced by the Presence of Along-Coast Estuaries

**S. N. Giddings**[1] **and P. MacCready**[2]

[1]Scripps Institution of Oceanography, University of California San Diego, La Jolla, CA, USA, [2]School of Oceanography, University of Washington, Seattle, WA, USA

**Key Points:**
- Remote coastal winds alter estuarine circulation direction
- Coastal upwelling enhances estuarine exchange flow while downwelling reduces/reverses exchange
- River plumes from neighboring estuaries can reverse estuarine circulation during downwelling conditions

**Correspondence to:**
S. N. Giddings,
sgiddings@ucsd.edu

**Citation:**
Giddings, S. N., & MacCready, P. (2017). Reverse estuarine circulation due to local and remote wind forcing, enhanced by the presence of along-coast estuaries. *Journal of Geophysical Research: Oceans*, *122*, 10,184–10,205. https://doi.org/10.1002/2016JC012479

Received 28 OCT 2016
Accepted 8 NOV 2017
Accepted article online 30 NOV 2017
Published online 29 DEC 2017

**Abstract** Estuarine exchange flow governs the interaction between oceans and estuaries and thus plays a large role in their biogeochemical processes. This study investigates the variability in estuarine exchange flow due to offshore oceanic conditions including upwelling/downwelling, and the presence of a river plume offshore (from a neighboring estuary). We address these processes via numerical simulations at the mouth of the Salish Sea, a large estuarine system in the Northeast Pacific. An analysis of the Total Exchange Flow indicates that during the upwelling season, the exchange flow is fairly consistent in magnitude and oriented in a positive (into the estuary at depth and out at the surface) direction. However, during periods of downwelling favorable winds, the exchange flow shows significantly more variability including multiple reversals, consistent with observations, and surface intrusions of the Columbia River plume which originates 250 km to the south. Numerical along-strait momentum budgets show that the exchange flow is forced dominantly by the pressure gradients, particularly the baroclinic. The pressure gradient is modified by Coriolis and sometimes advection, highlighting the importance of geostrophy and local adjustments. In experiments conducted without the offshore river plume, reversals still occur but are weaker, and the baroclinic pressure gradient plays a reduced role. These results suggest that estuaries along strong upwelling coastlines should experience significant modulation in the exchange flow during upwelling versus downwelling conditions. Additionally, they highlight the importance of nearby estuaries impacting one-another, not only in terms of connectivity, but also altering the exchange flow.

**Plain Language Summary** Estuarine systems provide extensive biological and ecological functions as well as contribute to human uses and economies. However, estuaries are susceptible to change and most estuaries have been significantly impacted, threatening their important functionality. Understanding estuarine dynamics is critical to understanding estuarine ecosystems. Hydrodynamic connectivity between estuaries and the coastal ocean is a key dynamical driver impacting critical biological and biogeochemical processes such as ocean/estuarine nutrient and phytoplankton exchange and regulation of estuarine residence time, dissolved oxygen, and acidification levels. Typically estuarine-ocean exchange brings oceanic water into the estuary at depth, mixes it upwards within the estuary, and returns an outflowing mixture of oceanic and riverine water at the surface to the ocean. This manuscript documents seasonal reversals to this typical circulation pattern and the hydrodynamic drivers of the reversals. It highlights the importance of offshore winds and connectivity with neighboring estuaries. Improved understanding of these mechanisms can help us predict how estuaries will respond to a changing climate.

## 1. Introduction

Estuarine systems provide extensive biological and ecological functions (e.g., McLusky & Elliott, 2004) as well as contribute to human uses and economies (e.g., Pendleton, 2008). However, estuaries are susceptible to change and most estuaries have been significantly impacted, threatening their important functionality. Understanding estuarine dynamics is critical to understanding estuarine ecosystems. Hydrodynamics influence transport of contaminants, nutrients, and larvae; morphology; and environmental conditions for organisms. Connectivity between estuaries and the coastal ocean is a key dynamical driver impacting critical biological and biogeochemical processes, such as ocean/estuarine nutrient and phytoplankton exchange (e.g., Boyer et al., 2002; Davis et al., 2014), and regulation of estuarine residence time, hypoxia,

and acidification (e.g., O'Callaghan et al., 2007). Additionally, connectivity between along-coast (i.e., neighboring or nearby) estuaries controls larval transport and population connectivity (e.g., McConnaughey et al., 1994; Yamada & Kosro, 2010).

Residual circulation, also known as the tidally averaged/subtidal circulation or estuarine exchange flow, governs this exchange between the ocean and the estuary and thus plays a large role in influencing these biological and biogeochemical processes. The goal of this paper is to investigate the variability in estuarine exchange flow due to offshore oceanic conditions including upwelling/downwelling, and the presence of a river plume (from a nearby, along-coast estuary) at the mouth of the very large, ecologically and economically important Northeast Pacific estuary: the Salish Sea. Following the introduction, we describe the numerical model in sections 2.1 and 2.2 and the numerical experiments and analysis techniques in sections 2.3. Importantly, we are using state-of-the-art numerical modeling and diagnostic analysis tools including realistic numerical simulations for 2004–2007 that incorporate passive dye tracers (section 2.3.2) and output diagnostic momentum terms (section 2.3.4) both with and without the forcing of a major river (section 2.3.1). Postsimulation analysis tools included particle tracking, calculations of the Total Exchange Flow (section 2.3.3), and a momentum budget (section 2.3.4). The results presented include along-coast connectivity (section 3.1), the exchange flow variability and drivers (section 3.2), and the influence of an offshore large river plume (section 3.3). Finally, we summarize the results and their applicability to other estuarine systems located along upwelling coastlines in section 4.

### 1.1. Estuarine Dynamics—Local Forcing

The subtidal dynamics of well-mixed and partially-mixed estuaries have generally been explained in terms of subtidal force balances (e.g., Hansen & Rattray, 1965; MacCready & Geyer, 2010; Pritchard, 1954, 1956), i.e., residual circulation and upstream salt fluxes are typically thought of as being dominated by gravitational circulation resulting from a balance of baroclinic and barotropic forcing, and mixing of momentum (the vertical divergence of Reynolds stress) associated with the barotropic tides. This results in a small net outflow of water due to the barotropic forcing from the river and a larger baroclinic exchange flow into the estuary at depth and out of the estuary at the surface (Chatwin, 1976; Hansen & Rattray, 1965), hereafter referred to as the traditional estuarine exchange direction. Alternatively, estuaries with strong stratification and/or topographic constrictions or sills can exhibit hydraulic control, whereby advection (rather than eddy viscosity) balances the pressure gradients (e.g., Armi & Farmer 1986; Stommel & Farmer, 1953). This balance has been shown to apply to deep fjords with sills and strong stratification (e.g., Arneborg et al., 2004) as well as shallow but strongly stratified estuaries (e.g., Geyer & Ralston, 2011). As highlighted by Hetland (2010), realistic estuaries have a complex blend of these momentum balances (pressure gradients, eddy viscosity, and advective terms) but most will likely behave more like a viscous estuary.

Although this simple model often describes observed residual circulation profiles well, additional forcing mechanisms, both local and remote, can drive the exchange flow and/or lead to temporal and spatial variability in the exchange flow. Past studies have explored the importance of unsteadiness (e.g., Kranenburg, 1986; MacCready, 2007), nonlinearities, direct wind forcing (e.g., Scully, 2010; Wang & Elliot, 1978), bathymetric complexity (e.g., Scully & Friedrichs, 2007; Valle-Levinson et al., 2000), and tidal dynamics such as asymmetries in mixing (Jay & Musiak, 1996; Jay & Smith, 1990) influencing residual circulation, reviewed in Geyer and MacCready (2014). These local forcing mechanisms can induce event scale, fortnightly, and seasonal variability in exchange flow (e.g., Bowen & Geyer, 2003; Stacey et al., 2001). Finally, in large estuaries, Coriolis can become an important force acting to adjust the flow structure (e.g., Valle-Levinson, 2011).

### 1.2. Estuarine Dynamics—Remote Forcing

In addition to these local mechanisms, remote forcing mechanisms can be important. Here we refer to "remote" forcing as forcing offshore of the estuary mouth including offshore river plumes (e.g., Banas et al., 2004, Figure 3f; Wong & Lu, 1994), coastal-trapped waves (e.g., O'Callaghan et al., 2007), and wind-driven upwelling/downwelling that alter conditions at the estuary mouth and thus can strongly impact estuarine exchange flow (e.g., Klinck et al., 1981; Stigebrandt, 1990). Some of these mechanisms may be understood in the context of classical estuarine exchange (i.e., exchange driven by the pressure gradient balanced by the vertical stress divergence, with turbulence driven by the tides, such that the exchange flow scales with the baroclinic pressure gradient, e.g., MacCready & Geyer, 2010). For example, upwelling conditions lead to increased salinity at the ocean boundary, a higher along-stream baroclinic gradient, and thus stronger

exchange flow (e.g., Hickey et al., 2002). In contrast, relaxation or downwelling reduces the along-estuary baroclinic gradient, reducing exchange flow. Similarly, the salinity at the mouth can be influenced by plume water from a neighboring alongshore estuary (e.g., Thomson et al., 2007; Wong & Lu, 1994). The dynamics are often more complex, with both baroclinic and barotropic forcing playing a role. An example is the sea surface elevation setup and Ekman flow associated with upwelling and downwelling conditions (e.g., Gilcoto et al., 2007; Valle-Levinson, 1995; Wang & Elliot, 1978). These types of remote forcing mechanisms, particularly the importance of offshore wind-driven circulation, have been highlighted in the fjord literature where pycnocline displacement offshore drives circulation within the fjord and has been termed "intermediary water exchange" (e.g., Aure et al., 1996) or "baroclinic pumping" (e.g., Arneborg, 2004) and is often modeled with simple two-layer box models (e.g., Gustafsson, 2000; Klinck et al., 1981; Stigebrandt, 1990).

The strong impact of oceanic variations on estuarine exchange has been observed to influence estuarine ecology including nutrient availability, productivity, and dissolved oxygen among others. Estuaries adjacent to upwelling regions often receive oceanic inputs of nitrogen impacting productivity (Monteiro & Largier, 1999; Newton & Horner, 2003; Roegner et al., 2011). Subtidal sea surface elevation changes due to coastal-trapped waves observed in the Swan River Estuary, Australia led to salinity intrusions associated with upstream movement of anoxic water and fish kills (O'Callaghan et al., 2007). A shift in offshore upwelling conditions has even been correlated with a large-scale, long-term trophic cascade in San Francisco Bay (Cloern et al., 2007). Better understanding of remote forcing mechanisms on estuarine dynamics will improve our understanding of these ecological impacts.

### 1.3. Northeast Pacific Ocean Coastal Estuaries and Oceanography

The Northeast Pacific coast is part of the eastern Pacific Ocean boundary California Current System (CCS) that exhibits currents with strong synoptic, seasonal, and interannual variability (Hickey, 1979, 1989). The California Current flows equatorward year-round offshore of the shelf and slope. The poleward California Undercurrent flows northward (except during Spring) over the continental slope, bringing nutrient rich, oxygen deplete southern source water that is raised onto the shelf during upwelling (e.g., Thomson & Krassovski, 2010). The Davidson Current flows northward during the winter, replacing the California Current in the 100 km closest to the coast. Currents over the shelf are typically in the same direction as the wind, i.e., southward during the summer and fall and northward during the winter and spring. Large-scale changes in the wind field create a dramatic spring transition when upwelling begins (Hickey, 1979) and high productivity ensues (Hickey & Banas, 2003). Another important feature is the influence of remote winds that leads to coastal-trapped waves that propagate northwards (Battisti & Hickey, 1984; Connolly et al., 2014).

Many estuarine systems line the Northeast Pacific coast. The two largest estuaries are the Salish Sea and the Columbia River. Similar large-scale atmospheric forcing patterns and interannual variability in upwelled source water, the timing of the spring transition, and the magnitude and persistence of upwelling-favorable and downwelling-favorable winds drive the interannual variability in oceanic conditions observed at the estuary mouths. In addition to a strong upwelling regime dominating impacts at the their mouths, Northeast Pacific estuaries experience dramatic seasonal variability in freshwater input and strong tides.

As a result of the strong variability in forcing both at the mouth and upstream, Northeast Pacific estuaries exhibit strong synoptic, seasonal, and interannual variability in estuarine exchange flow. Of the smaller regional estuaries, Willapa Bay has been studied most extensively. Upwelling (often coincident with low riverine flows) modifies the along-channel density gradient producing enhanced exchange flow. The opposite occurs during downwelling events, and in addition intermittent Columbia River (CR) plume intrusions occur (Banas et al., 2004; Hickey & Banas, 2003; Hickey et al., 2002; Roegner et al., 2002). This estuary exhibits unsteady exchange flow due to the influence of these remote forcing events at synoptic time scales (Banas et al., 2004; Hickey & Banas, 2003). The importance of upwelling was also observed in other Northeast Pacific estuaries including Grays Harbor (Duxbury, 1979; Hickey & Banas, 2003), Yaquina Bay (Brown & Ozretich, 2009) and the Alsea estuary (de Angelis & Gordon, 1985).

The river plumes emanating onto the Northeast Pacific coast also experience variability due to large-scale atmospheric forcing conditions. Plumes tend offshore and southward during upwelling conditions and northward along the coast during downwelling conditions as expected (Fong & Geyer, 2001, 2002; Hickey et al., 2005). The CR plume, the largest plume in the region, is known to reach all the way to the Strait of Juan de Fuca (hereafter referred to as the Strait) and interact with the outflow from the Salish Sea.

Observations by Thomson et al. (2007), Hickey et al. (2009), Holbrook and Halpern (1982), and Frisch et al. (1981) suggest that CR plume water intrudes into the Strait during some downwelling periods. These alongcoast plume interactions impact regional circulation both along and across the shelf (Banas et al., 2009a; Giddings et al., 2014; Hickey et al., 2009).

This manuscript focuses on the exchange flow of the Salish Sea, which can be viewed as a large estuary with its mouth being the Strait of Juan de Fuca, which connects the large inland water body to the Pacific Ocean. The Salish Sea fjord system contains deep, steep walls, and a multitude of riverine inputs. These rivers mix extensively with oceanic water within the Salish Sea before reaching the Strait, such that the volume-averaged baroclinic pressure gradient (divided by density) along the strait is relatively small, at most $-2 \times 10^{-5}$ m s$^{-2}$ (i.e., salinity varies by $<$2 psu over the $\sim$100 km long Strait). As a highly productive estuary with significant ecological and human resources, understanding its connectivity with the Pacific Ocean is critical.

Observations within the Strait have shown complex circulation that sometimes deviates from a traditional estuarine exchange flow (e.g., Cannon, 1978; Frisch et al., 1981; Holbrook et al., 1980; Holbrook & Halpern, 1982; Thomson et al., 2007). During the upwelling season, there is a well-established exchange flow (into the estuary at depth, out at the surface), however it does not always encompass the entire water column. Deeper than this exchange flow, a third layer flowing outward sometimes occurs. During downwelling favorable winds, the exchange flow has been shown to occasionally reverse, becoming inward at the surface. This reversal has been named the Washington Counter Current and researchers have speculated on its origin (Hickey et al., 2009; Holbrook & Halpern, 1982; Thomson et al., 2007), some hypothesizing the importance of downwelling and of the Columbia River plume in these events. Local forcing of the Salish Sea exchange due to, for example, low river flow during drought (Newton et al., 2003) and fortnightly modulation of tidal mixing (Hickey et al., 1991; Masson & Cummins, 2000), has been well documented. While there is evidence that subtidal variability of hydrographic conditions within the Salish Sea is in part due to remote climate forcing, the relative importance of local versus remote forcing is somewhat unclear, varying by location and method (Babson et al., 2006; Martin & MacCready, 2011; Moore et al., 2008).

Here we use numerical simulations of the region including the Salish Sea, the Pacific Ocean, and the Columbia River to examine the temporal variability in the exchange flow through the Strait. The study has obvious implications for the Northeast Pacific region but also relevance to other estuaries located along strong upwelling zones (e.g., Banas et al., 2004; Monteiro & Largier, 1999) and/or influenced by a nearby river plume (e.g., Banas et al., 2004; Li et al., 2011; Wong & Lu, 1994). An important subset of estuaries for which this study applies is fjords. For example, the fjords in Greenland and Norway have been shown to respond strongly to coastal dynamics altering their circulation (e.g., Aure et al., 1996; Jackson et al., 2014; Stigebrandt, 1990; Straneo & Cenedese, 2015; Sutherland et al., 2014). Specifically we will address the relative role of remote forcing mechanisms on the Strait of Juan de Fuca exchange flow including the impact of the large neighboring Columbia River.

## 2. Methods

### 2.1. Model Setup and Forcing Parameters

The numerical simulations use the Cascadia domain and modeling framework developed by the University of Washington Coastal Modeling Group (UWCMG) (Banas et al., 2009a; Liu et al., 2009a, 2009b; MacCready et al., 2009; Sutherland et al., 2011). The model used here is described in detail in Giddings et al. (2014), including extensive validation against observations. The modeling framework employs the Regional Ocean Modeling System (ROMS) (Shchepetkin & McWilliams, 2005), a free surface, hydrostatic, primitive equation model. The models are initialized with realistic oceanic flows and forced with realistic atmospheric forcing, tides, river flow, and ocean boundary conditions to conduct hindcast simulations of the hydrodynamic conditions throughout the domain. The final simulations were run with the addition of a biogeochemical model (NPZDO, see, Davis et al., 2014 and Siedlecki et al., 2015), five passive tracers, and diagnostics.

Figures 1h and 1i include the river flow and winds over the full 4 years (2004–2007) of simulation for reference. These years include some interannual variability. For example, 2005 and 2006 had stronger upwelling relative to 2004 and 2007, which exhibited weaker upwelling winds with intermittent relaxation/downwelling events. 2005 exhibited a delayed spring transition (delayed onset of upwelling) (Kosro et al., 2006).

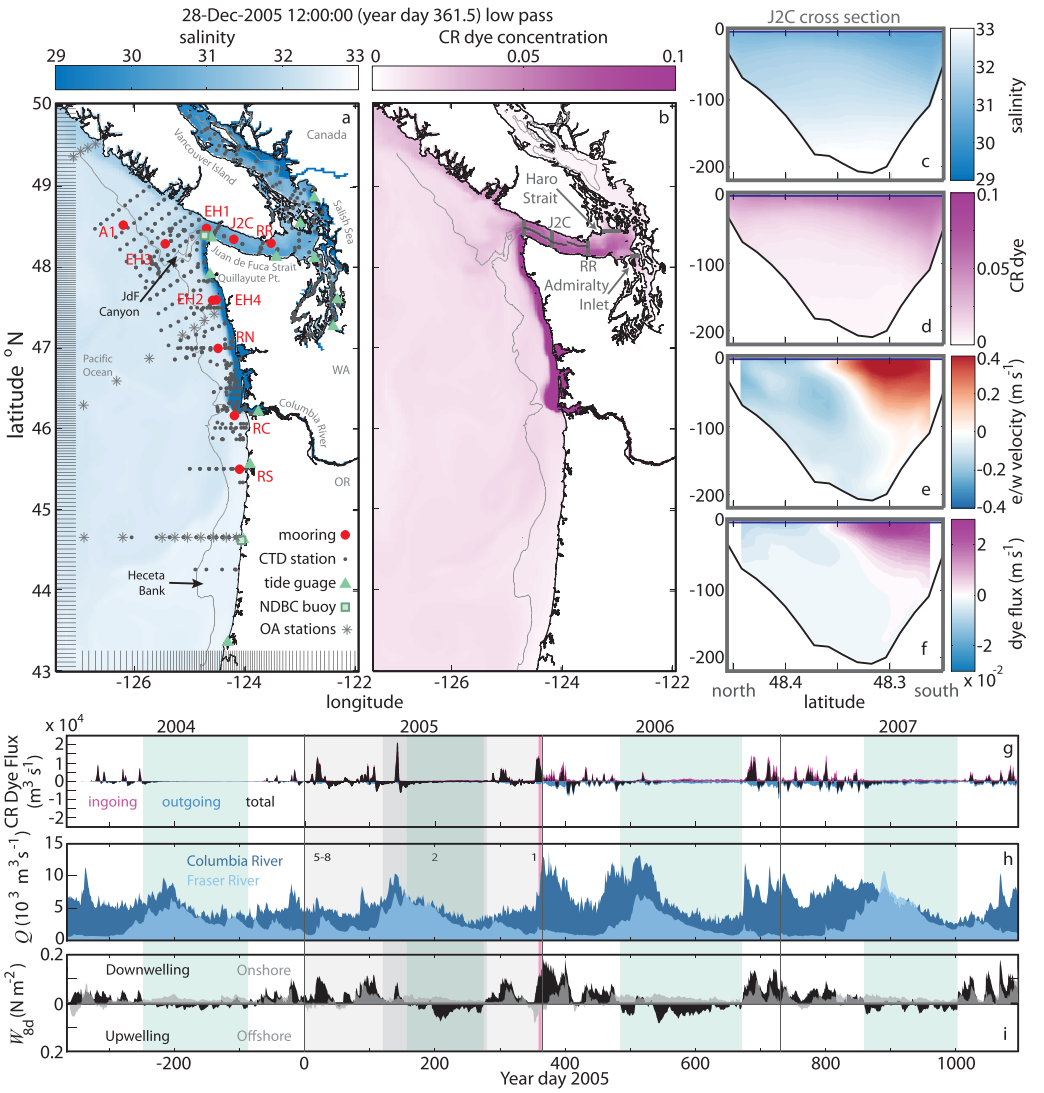


**Figure 1.** Model snapshots and simulation period. Low pass (Godin filter, Emery & Thomson, 2004) (a) surface salinity, (b) surface Columbia River (CR) dye concentration, and (c–f) cross sections through the Strait of Juan de Fuca at location J2C on 28 December 2005 during a strong downwelling-favorable wind. Cross sections include (c) salinity, (d) CR dye concentration, (e) east/west velocity (m $s^{-1}$), showing a reversed exchange flow, and (f) dye flux (m $s^{-1}$). Note that the passive dye tracer is unit-less, but mixes similarly to salinity and temperature and enters the domain at the head of the CR with a concentration of 1. Bottom plots show the full 4 year simulation period including (i) the 8 day weighted mean wind stress (exponentially decaying running mean) computed as described in Austin and Barth (2002), but employed as a filter to retain the units of stress (see Giddings et al., 2014); positive is downwelling favorable for the N/S (black) winds and toward the shore for the E/W (gray) winds, (h) river flows in the Columbia (dark blue) and Fraser (light blue) Rivers, and (g) the integrated dye flux through the cross section ($m^3$ $s^{-1}$) split into ingoing (pink), outgoing (blue), and total (black) fluxes. The time period for the top plots is marked on the bottom plots as a pink line. The time period for Figures 2 and 5−8 are also indicated in gray shading. Note that the approximate upwelling season is highlighted in light green for each year. Tick marks on the axes of (a) indicate every other grid point. One hundred and eighty meters bathymetry contour on (a) and (b) is near the shelf-break.

2004–2005 and 2006–2007 were weak El Niño events. Example snapshots of simulated surface salinity and cross sections through the Strait of Juan de Fuca during downwelling are shown in Figures 1a–1f.

### 2.1.1. Domain

The Cascadia domain extends from 43°N to 50°N and out to 127.4°W encompassing the inland waters of the Salish Sea (which includes Puget Sound, the Strait of Georgia, and the Strait of Juan de Fuca) and the coastal ocean and estuaries of WA, OR, and Vancouver Island (VI), British Columbia (see Figure 1). The final model resolution from which results are presented stretches from 1.5 km within the Salish Sea and at the

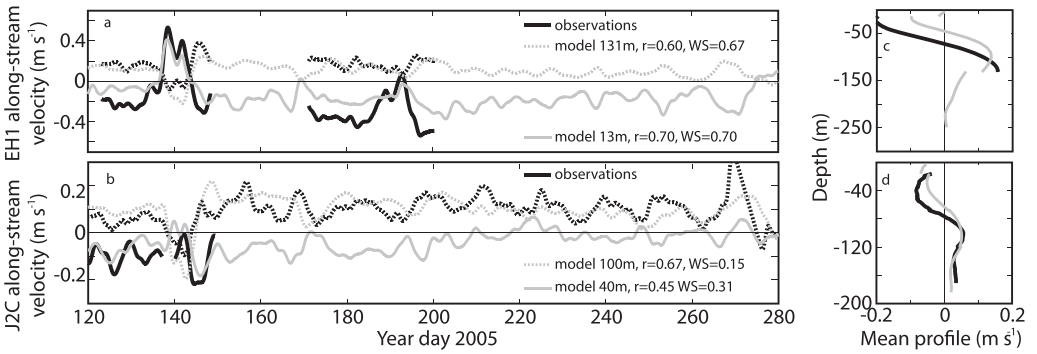


**Figure 2.** Validation of exchange flow within the Strait of Juan de Fuca. (a and b) subtidal along-Strait velocity near the surface (solid) and near the bottom (dashed) at two locations in the center of the Strait of Juan de Fuca (a, EH1 and b, J2C, both marked in Figure 1). Note that the near-surface and near-bottom depths were chosen based on the observed maximum mean inflow and outflow depths. (c and d) mean subtidal along-Strait velocity over the observational record period in 2005 at the same two locations in the center of the Strait (c, EH1 and d, J2C) over depth. Along-Strait velocity is determined by principle axes analysis and subtidal currents are calculated using a Godin filter (Emery & Thomson, 2004). On all plots observations are in black, simulation outputs are in gray, and correlation coefficients (*r*) as well as Willmott Skill Scores (*WS*) (Willmott, 1982) are displayed.

Coast to 4.5 km offshore and has 40 vertical S levels with enhanced near-bottom and near-surface resolution. Grids with higher resolution performed comparably (described briefly below). This grid was chosen as it was the most computationally efficient while maintaining adequate representation of the relevant physical processes.

### 2.2. Model Validation

Model validation, particularly along the coast as well as of the Columbia River plume variability is covered extensively in Giddings et al. (2014), thus here we focus on model validation of the exchange flow through the Strait of Juan de Fuca.

#### 2.2.1. In Situ Observations

Simulated along-Strait subtidal velocities show reasonable skill compared to observations (Figure 2). For most of the time series presented in Figure 2, the flow is in the direction expected of a traditional exchange flow (into the estuary at depth and out near the surface). Note that the time series presented in Figure 2 is during the upwelling season (winter observations are difficult to make inside the Strait, although a few are shown in Thomson et al., 2007 and Holbrook and Halpern, 1982). The record does contain one strong reversal event around day 140 (21 May 2005) close to the spring transition. The subtidal velocities capture the mean residual vertical profile well (Figures 2c and 2d) and the time-variation (Figures 2a and 2b), although the model near-surface outflow is too weak at EH1.

Additional in situ observations (moorings and CTD casts) along the Oregon coast as well as satellite observations confirm the temporal and spatial variability in the simulated Columbia River plume and coastal upwelling with good skill (see Giddings et al., 2014 for more validation).

#### 2.2.2. Resolution Tests

We compared several different model grids to ensure that the exchange flow through the Strait of Juan de Fuca was well resolved. Both a higher and lower resolution grid was described and compared in Giddings et al. (2014), showing that the grid we present here and the higher resolution grid compare favorably. In addition to those prior tests, we also created a grid that had enhanced resolution within the Salish Sea (400 m). While the 400 m resolution within the Salish Sea improved representation of fine scale bathymetry and physics within the Salish Sea, performance with regards to the exchange flow through the Strait was statistically similar and the momentum budget analysis resulted in similar findings. The final grid used here maintains the strength and variability of the exchange flow, coastal processes, and momentum balance as the higher resolution test grids, but with improved computational efficiency.

### 2.3. Model Experiments and Analysis Tools

Here we describe the various model experiments and analysis tools that we employ to investigate the exchange flow in section 3. Model simulations are completed for 2004–2007 incorporating passive dye

tracers (section 2.3.2) and output diagnostic terms (section 2.3.4) both with and without the Columbia River (section 2.3.1). Postsimulation analysis tools included calculations of the Total Exchange Flow (section 2.3.3), and a momentum budget (section 2.3.4).

#### 2.3.1. CR on and CR off (noCR)

In order to test the hypothesis that the Washington Counter Current is the Columbia River reaching the mouth of the Strait of Juan de Fuca, we ran simulations without the Columbia River (noCR) by replacing the river mouth with a coastal wall and removing the freshwater input (e.g., see Banas et al., 2009b; Giddings et al., 2014). Everything else in the noCR runs was identical to the full simulations.

#### 2.3.2. River Dye Tracers

Passive dye tracers within ROMS are used to track the different freshwater sources in the domain. Three different dye tracers are used to track the Columbia River, Fraser River, and the remaining Salish Sea rivers separately. They enter at the river mouths at a concentration of 1. They mix similarly to salinity and potential temperature, thus tracking the freshwater sources separately.

#### 2.3.3. Total Exchange Flow (TEF)

To quantify exchange flow through the Strait, we use the Total Exchange Flow (TEF) method described in MacCready (2011). There are many methods to calculate exchange flow in estuarine systems (see Geyer & MacCready, 2014, for a recent summary) with differing interpretations. TEF calculates exchange flow in an isohaline coordinate and has the advantage of incorporating both subtidal and tidal fluxes (Chen et al., 2012) and exactly satisfying the Knudsen relationship (Knudsen, 1900; MacCready, 2011; MacCready & Geyer, 2010).

#### 2.3.4. Diagnostics and Momentum Budgets

The simulations for 2005 (both with and without the Columbia River) were rerun with the ROMS diagnostic terms enabled, which provide the terms in the momentum budget averaged over the hour between model field saves. Exporting the diagnostic terms allows for a full momentum balance to be calculated and closed over the full model domain and throughout time. Momentum budgets are calculated along the Strait to determine the important driving dynamics for the exchange flow.

## 3. Results

### 3.1. Along-Coast Connectivity

The dye tracers clearly show the strong connectivity between the Columbia River and the WA coastal estuaries (e.g., Figure 1). The Columbia River dye hugs the coast and moves northwards during downwelling as previously observed (Hickey et al., 2005, 2009). During strong and/or extended periods of downwelling, the plume makes it to the mouth of the Strait and can intrude into the Strait as suggested by prior observations (e.g., Hickey et al., 2009) and shown in a snapshot in Figure 1. The passive dye tracer shows the dye reaching as far inland as Vancouver, Canada and throughout Puget Sound at concentrations of 0.02 (2% of the incoming CR value), and Orcas and Whidbey Islands at concentrations of 0.04. This suggests that CR water could be responsible for freshwater signals observed at Friday Harbor during times when the Fraser River plume is pushed northward by winds (J. Newton, personal communication, 2012) and suggests a mechanism to bring a mixture of CR and coastal surface water, and associated organisms, into the Salish Sea surface waters.

Maximum CR dye concentrations observed at the mouth of the Strait are nearly 0.3 (30% of the incoming CR value). These values decrease to less than 10% near Race Rocks (RR in Figure 1) and remain at approximately that value at the entrances of the Strait of Georgia (Haro Strait) and Puget Sound (Admiralty Inlet) (see Figure 1 as an example, full analysis not shown). As a comparison, maximum Fraser River dye concentrations are nearly 35% at Haro Strait (the main conduit for Fraser River water to exit the Strait of Georgia toward the ocean), just above 20% near Race Rocks, and around 10% at the mouth of the Strait. The dye concentrations give an idea where mixing of river water with ambient ocean water occurs. The largest % decreases in the median CR dye concentration ($>$80% decreases) are within the CR estuary and again along the Strait of Juan de Fuca (more % decrease than along the open coast). Similarly FR dye concentrations decrease dramatically both along Haro Strait (median $>$90% decrease) as well as along the Strait of Juan de Fuca (median $>$60% decrease). This indicates a significant amount of mixing within the estuaries and along the Strait of Juan de Fuca. High mixing at the CR mouth is expected because of the estuarine dynamics and plume liftoff (e.g., Horner-Devine et al., 2015; MacCready et al., 2009). High mixing along the Straits,

particularly towards the Strait of Juan de Fuca's eastern end, matches with prior observations of the Salish Sea being a weakly stratified estuary with strong tidal currents, steep bathymetry and sills that encourage vertical mixing (e.g., Griffin & Leblond, 1990; Herlinveaux & Tully, 1961; Masson & Cummins, 2000).

Time series of dye fluxes through the Strait (see Figure 1g) indicate that CR water enters the Strait ~60% of the time over the years modeled, typically during downwelling favorable winds (which also occur ~60% of the time during the modeled years). Some of the dye that enters the Strait during these strong downwelling events exits at lower concentrations (due to mixing) as the winds relax and/or reverse. During individual intrusion events, such as that shown in Figure 1, cross sections through the Strait reveal a reversed exchange flow throughout the water column (Figure 1e) with water exiting the estuary at depth and entering the estuary at the surface. Strong lateral variability in this exchange is clear, with the inflowing surface water, high in CR dye, hugging the south side of the Strait. This qualitatively matches observations by Frisch et al. (1981), Holbrook and Halpern (1982), and Thomson et al. (2007) who observed surface water during reversals hugging the southern edge of the Strait and consisting of less dense water.

Particle tracking experiments (described in more detail in Giddings et al., 2014) show similar results with surface-trapped particles able to enter the Salish Sea during downwelling periods. A comparison between simulations with and without the Columbia River previously showed that the CR tends to block alongshore and onshore transport (Banas et al., 2009a; Giddings et al., 2014) except during large downwelling events when particles are entrained into the plume (Giddings et al., 2014). In the case of downwelling + entrainment, the CR plume can act as a conduit enhancing northward alongshore transport. Tracking these particles into the Salish Sea, similarly, the presence of the CR enhances the ability for surface-trapped particles to enter the Salish Sea during downwelling. This holds true regardless of whether particles originated in the plume or outside of the plume in open ocean waters, so long as they were entrained into the plume. This transport pathway indicates enhanced estuary-to-estuary and surface ocean-estuary connectivity during downwelling. This is important as it suggests a mechanism for near-surface oceanic waters to enter the Salish Sea (not possible during the upwelling season) and is a potential explanation for the observed presence of oceanic species of phytoplankton in the Salish Sea (e.g., Holbrook et al., 1980). It also shows significant intermingling of different estuaries that could similarly be important for larval, nutrient, or pollutant transport.

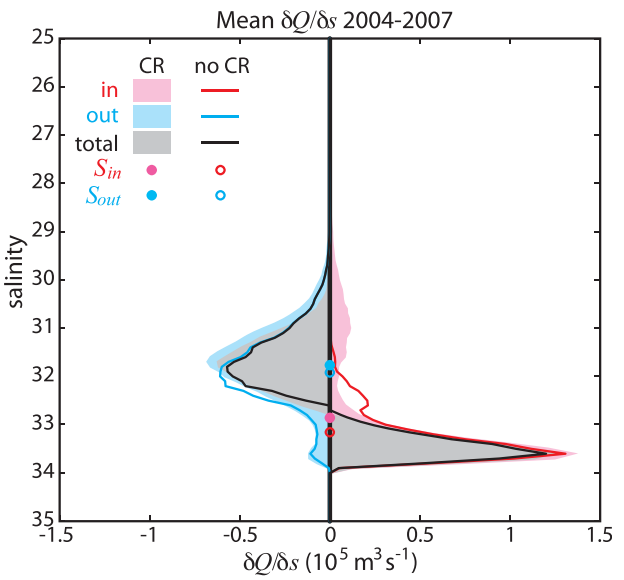


**Figure 3.** Mean total exchange flow. Mean incoming (reds), outgoing (blues), and total (black) exchange flow for the full simulations (shaded) and noCR simulations (lines) over the full 4 years of simulation (2004–2007) at the center of the Strait (J2C, location marked in Figure 1). The mean incoming and outgoing salinity values are marked with dots (open dots are for the noCR simulation).

### 3.2. Exchange Flow

Applying TEF to multiple sections along the Strait of Juan de Fuca shows relatively consistent seasonal and along-strait patterns. The mean TEF over the 4 year simulation period indicates incoming flow at high salinity and outgoing flow at lower salinity (see Figure 3, gray). Splitting TEF into the incoming and outgoing components reveals a small amount of flow entering at lower salinities (pink bump ~31.5 psu in Figure 3) and exiting at higher salinity (light cyan bump ~34 psu in Figure 3) indicative of occasional exchange reversals. The mean incoming and outgoing salinities (dots in Figure 3) are just above 1 psu different from one-another indicating a weakly stratified estuary. Applying the steady Knudsen's relationship with the mean Salish Sea river flow ($Q_r = 3.8 \times 10^3$ m$^3$ s$^{-1}$) and mean incoming and outgoing salinities through the Strait, the exchange flow, $Q_{in}$ is estimated at $\sim 1 \times 10^5$ m$^3$ s$^{-1}$ = 0.1 Sv, nearly 30 times greater than the river flow such that $Q_{in} \sim = Q_{out}$. This is equivalent to that calculated using TEF, which is necessary as TEF satisfies the Knudsen relationship. It is important to note that our estimates of $Q_{in}$ match those calculated from numerical simulations with a much more highly resolved Salish Sea (Sutherland et al., 2011) and are similar to those estimated from prior observations and numerical models over a range of sampling periods (see Table 1, Foreman et al., 2000; Godin et al., 1981; Labrecque et al., 1994; Masson & Cummins, 2000; Thomson et al., 2007).

**Table 1**
*Exchange Flow Comparisons*

| Study | Model or obs? | Location | Time period | *Qr* (*Sv*) | *Qin* (*Sv*) | *Qout* (*Sv*) |
|---|---|---|---|---|---|---|
| Giddings et al. (this study) | Model | J2C | 1 year average, 2005 | 0.004 | 0.11 | 0.11 |
| Giddings et al. (this study) | Model | J2C | 1 year 2005 minimum, normal exchange | 0.002 | 0.01 | 0.02 |
| Giddings et al. (this study) | Model | J2C | 1 year 2005 maximum, normal exchange | 0.012 | 0.20 | 0.21 |
| Sutherland et al. (2011) | Model | J2C | 1 year average, 2006 | 0.001 | 0.12 | 0.12 |
| Thomson et al. (2007) | Observations | J2C | 3 year average May 2002 to May 2005 | 0.005–0.015* | 0.09 | 0.11 |
| Masson and Cummins (2000) | Model | Midstrait, near J2C | Forced with early summer values, minimum | 0.005 | 0.15 | 0.15 |
| Masson and Cummins (2000) | Model | Midstrait, near J2C | Forced with early summer values, maximum | 0.005 | 0.20 | 0.20 |
| Labrecque et al. (1994) | Observations | Midstrait, near J2C | 40 day average, summer 1975, 26 May to 5 July | 0.006* | 0.22 | 0.27 |
| Labrecque et al. (1994) | Observations | Mouth of strait, near EH1 | 40 day average, summer 1984, 20 June to 30 July | | 0.15 | 0.16 |
| Godin et al. (1981) | Observations | Midstrait, near J2C | 20 April to 10 May 1973 minimum | 0.003* | 0.09 | 0.09 |
| Godin et al. (1981) | Observations | Midstrait, near J2C | 20 April to 10 May 1973 maximum | 0.003* | 0.16 | 0.16 |
| Foreman et al. (2000) | Model | Midstrait, near J2C | Forced with summer averages from 1968 to 1999 | | 0.11 | 0.11 |

*Note.* This table summarizes multiple observational and modeling studies in the Strait of Juan de Fuca that estimate the incoming and outgoing volume fluxes (Foreman et al., 2000; Godin et al., 1981; Labrecque et al., 1994; Masson & Cummins, 2000; Sutherland et al., 2011; Thomson et al., 2007). In many studies, the river flow is estimated (demarcated with *). Most values are similar to the annual mean calculated in this study or fall within the minimum and maximum values of this study. One exception is Labrecque et al. (1994) whose 1975 estimate is high, but has been attributed to high runoff by Masson and Cummins (2000) and also was estimated from sparse measurements over a relatively short time period.

#### 3.2.1. Seasonal and Interannual Variability

Figure 4 shows TEF over the 4 year simulation period including the incoming flow ($Q_{in}$) and the salinity difference ($\Delta S = S_{in} - S_{out}$). During the upwelling-favorable summer/fall season the exchange flow is in the traditional direction and is relatively steady over time. During the downwelling-favorable winter/spring season, sometimes the exchange flow reverses ($\Delta S < 0$) and in general exhibits significantly more variability in both its strength and direction than during the upwelling season. The reversals are clearly correlated with downwelling-favorable winds (see section 3.2.2 for a quantitative analysis) and thus interannual variability in upwelling/downwelling wind strength and timing would be expected to play an important role. For example, large-scale oceanographic patterns such as ENSO or the PDO will impact the winds and thus manifest themselves in interannual variations to the estuarine exchange flow.

#### 3.2.2. Drivers of the Exchange Flow

We use a momentum balance to determine the dynamical force balance driving the exchange flow. ROMS diagnostic terms are analyzed at multiple along-Strait locations. For example, in Figure 5, a north-south cross section through J2C is included showing the mean across-section (east-west) velocity and density in the upper-left plot and mean east-west momentum terms in the following panels. The east-west direction is not aligned directly with the principle axes of the flow, however approximately represents the along-strait direction and is appropriate for the TEF and momentum analyses. The mean flow is "well-behaved" in the sense that it represents a typical exchange flow with near-surface flow exiting the estuary over the upper approximately 50 m (negative velocity) and a bottom layer entering the estuary (positive velocity) which is maximum around 100 m. The upper layer is tilted as expected due to geostrophy. Mean momentum terms through this same cross section suggest a predominance of the baroclinic pressure gradient (mean values $5.9 \times 10^{-6}$ m s$^{-2}$), although Coriolis, advection and the barotropic pressure gradient cannot be neglected (mean values $3.3–4.0 \times 10^{-6}$ m s$^{-2}$), whereas acceleration and vertical mixing are an order of magnitude smaller.

At different sections along the Strait, the balances are not always this simple. For example, at the mouth of the Strait (EH1, not shown), while the baroclinic pressure gradient remains dominant in driving the vertical flow structure, the Coriolis and advection terms are stronger and not in consistent directions. The total Coriolis term is strongly positive near the surface while the advection term is negative, in large part canceling the Coriolis effect. Even farther into the estuary at Race Rocks, the inflowing and outflowing streams become nearly horizontally separated rather than vertically, with Coriolis playing a critical role in this balance and the baroclinic pressure gradient actually reverses locally. The latter phenomena was documented in Martin and MacCready (2011) and named the Port Angeles Depression Dome, or PADD. More consideration of the along-Strait variability in the exchange flow and its drivers are in the following section

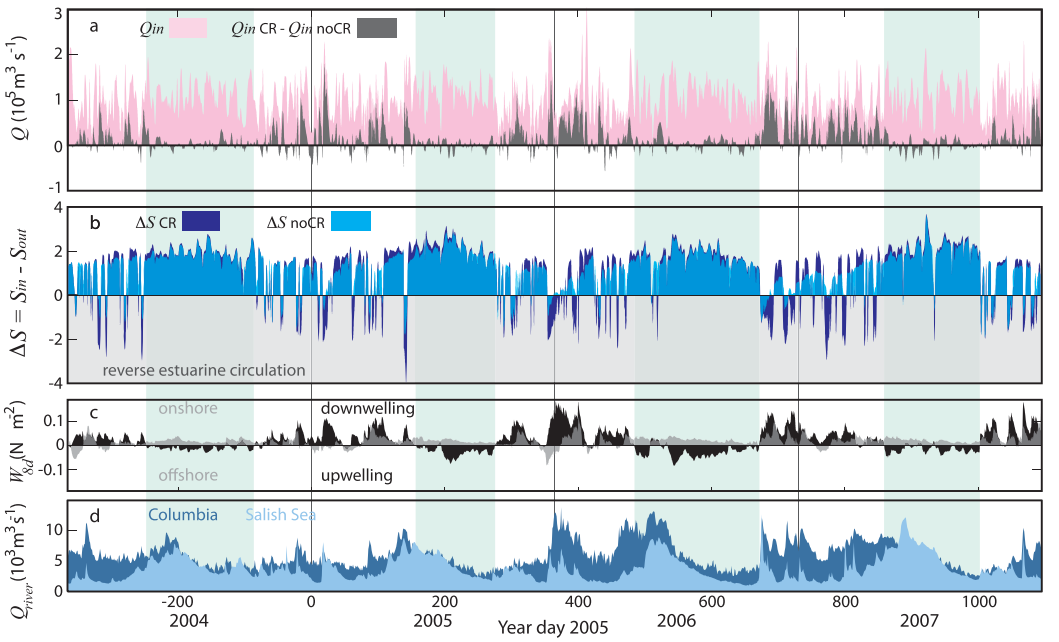


**Figure 4.** Total exchange flow over time. (a) Mean incoming (pink, $Q_{in}$) flow for the full simulation and the difference between the full simulation and the noCR simulation (gray). (b) Salinity difference ($\Delta S$ = mean incoming salinity, $S_{in}$—mean outgoing salinity, $S_{out}$) for the full simulation (dark blue) and noCR simulation (light blue). Note that if the incoming salinity is less than the outgoing, $\Delta S < 0$, the exchange flow must be reversed. (c) Principle axes cumulative winds where $>0$ is downwelling favorable (black) or onshore (gray). The 8 day weighted mean wind stress (exponentially decaying running mean) is computed as described in Austin and Barth (2002), but employed as a filter to retain the units of stress (see Giddings et al., 2014). Note that the approximate upwelling season is highlighted in light green for each year. (d) River flow from the two major river sources, the Columbia River and the Salish Sea (sum of all rivers entering the Salish Sea, where the Fraser River is the predominant, i.e., compare to Figure 1h).

(section 3.2.3), however far from the Strait entrance and exits, in the middle, the exchange flow and momentum balance look similar to those at J2C (Figure 5).

During reversed exchange flow the reversal manifests throughout depth with inflow at the surface and outflow at depth (Figure 6). The inflow is trapped near the surface toward the south and the isohalines slope in the opposite direction compared to typical exchange conditions. The momentum balance has similar dominant terms (with comparable magnitudes), however, importantly, the Coriolis and baroclinic pressure gradient terms have reversed vertical structure.

Despite along-stream variation in the balance due to local adjustments, we see a predominance of the pressure gradients, Coriolis force, and advection in the momentum balance (as seen in Figures 5 and 6) throughout most of the Strait similar to that suggested in a more idealized numerical analysis by Martin and MacCready (2011). The consistent, nearly equal and opposite, baroclinic pressure gradient and Coriolis force suggests the system is typically in geostrophic balance over the time scales analyzed here (subtidal and longer). Importantly, however this does not indicate what drives the exchange flow. To clarify this we investigate Coriolis + Advection + Pressure gradient terms (i.e., CAP from Martin and MacCready, 2011). As described by Martin and MacCready (2011), the goal of this formulation is to examine a Bernoulli-like term that smooths out effects of topography, i.e., CAP is the total pressure gradient modified by the gradient of momentum advection and the along-channel Coriolis force that can develop due to any misalignment of the (largely geostrophic) mean flow and the section normal direction relative to the principle axes of the flow.

Note that because the exchange flow swaps signs, in order to understand what drives the exchange flow (either positive of reverse), an average is only taken over the "spin-up" phase of that sign of exchange, which we approximate by the first half of the time period where the flow is in the direction of interest. Because some events are particularly long (for example, there is extended normal exchange flow during the summer upwelling season), this spin-up is capped at a maximum value of 8 days, which is a reasonable event time scale in this coastal region (e.g., Austin & Barth, 2002; Giddings et al., 2014, and others) and

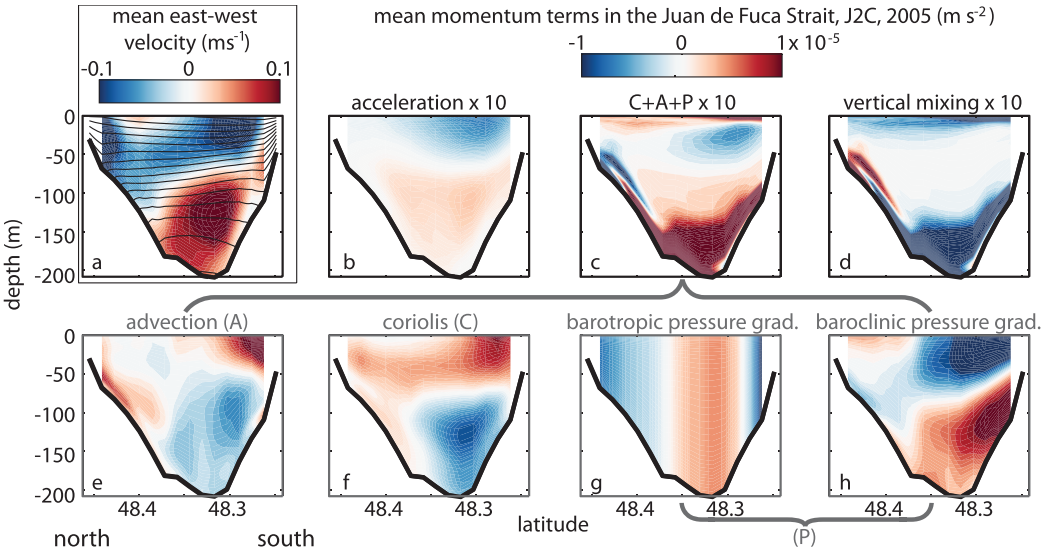


**Figure 5.** Mean east-west momentum terms in the center of the Strait of Juan de Fuca during normal exchange spin-up. (a) Mean east-west velocity (m $s^{-1}$, color where red indicates flow into the estuary and blue indicates flow out of the estuary) and density (black contours at 0.25 kg $m^{-3}$ intervals) at section J2C during the spin-up for normal exchange flow throughout 2005. Spin-up is defined as the first half of the time period normal exchange flow (defined by $\Delta S >= 0$) persists, capped at a maximum of 8 days. The remaining panels show the mean momentum budget terms (m $s^{-2}$) including (b) acceleration, (c) CAP (Coriolis + horizontal advection + vertical advection + total pressure gradient, i.e., sum of the bottom plots: (e + f + g + h), (d) vertical friction, (e) advection, (f) Coriolis, (g) barotropic pressure gradient, and (h) baroclinic pressure gradient. Note that the acceleration, CAP, and mixing terms on the top row are multiplied by 10 (i.e., they range over $\pm 1 \times 10^{-6}$ m $s^{-2}$ while those terms on the bottom row, that sum to equal CAP, range over $\pm 1 \times 10^{-5}$ m $s^{-2}$). Terms are arranged such that the acceleration term is on the left-hand side of the equation and all other terms are on the right-hand side such that positive momentum terms (red) will drive acceleration into the estuary and negative terms (blue) would drive acceleration out of the estuary. North is to the left on all plots such that these figures are facing into the estuary. Note that the principle axes direction at this cross section is $-20°$ and that the east-west velocity component is nearly the same as the along-stream velocity component.

results are not sensitive to the choice of this cap value. In reality, spin-up begins before the exchange flow swaps directions, but the starting and ending phase of the spin-up is difficult to identify. Nevertheless, this approximation clearly shows a nonzero acceleration in the direction of the exchange and thus highlights the mean terms driving that flow.

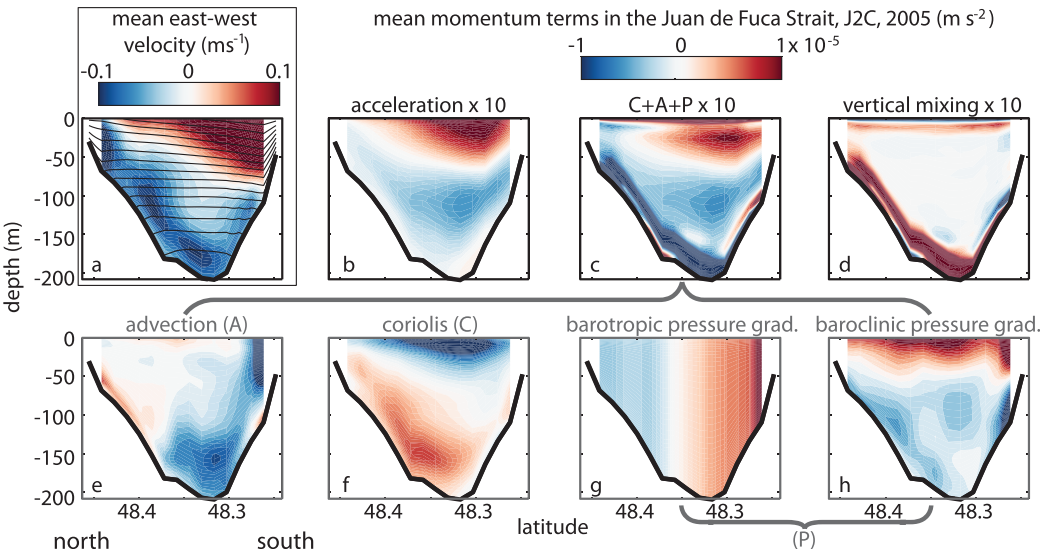


**Figure 6.** Momentum terms in the center of the Strait of Juan de Fuca during exchange reversal spin-up. Similar to Figure 5 but during reversed exchange flow spin-up only (determined by $\Delta S < 0$).

In both normal (Figure 5) and reverse (Figure 6) exchange conditions, we see that the acceleration leading to the observed exchange structure is dominated by CAP, and in particular the baroclinic pressure gradient portion of CAP. In other words, while CAP is an order of magnitude less than each of the terms that comprise it, its residual spatial structure which drives the acceleration (i.e., does not cancel with the vertical mixing term) results from the baroclinic pressure gradient term as can be seen from the cross sections in Figures 5 and 6. This indicates that the baroclinic pressure gradient does indeed drive the exchange flow as theory predicts. However, only a small portion of the total baroclinic forcing contributes to this acceleration, a significant portion of the baroclinic term is balanced by Coriolis (geostrophic adjustment) and advection (in part due to varying bathymetry driving local cross-channel flows and varying tidal currents as well as the orientation of the section relative to the principle axes flow direction).

Similar results are obtained if we complete a momentum balance in the TEF framework, i.e., calculate a mean momentum balance in salinity coordinates (rather than depth coordinates like above). In particular, high salinity water experiences a positive baroclinic pressure gradient and negative Coriolis forcing and low salinity water experiences a negative baroclinic pressure gradient and positive Coriolis forcing throughout the upwelling season (not shown). During the downwelling season, these forces can reverse sign indicative of a reversed pressure gradient driving the reversed exchange flow. Following Martin and MacCready's (2011) analysis, we step back and examine the exchange flow across the entirety of the Strait. If we compare the large-scale pressure gradient along the length of the strait (which we refer to as the "bulk" pressure gradient to differentiate it from the local pressure gradients shown in the momentum budget analyses, i.e., Figures 5 and 6) to the exchange flow at the center of the Strait, we find a statistically significant correlation between the exchange flow (TEF $Q_{in}$) and the bulk baroclinic pressure gradient ($r = -0.64$, $p = 0$) in the full simulation. Statistical significance here is defined as $r$ being different from 0 within 95% confidence intervals using a $z$ test (where Pearson's $r$ is converted to Fisher's $z'$). Martin and MacCready's (2011) analysis focused only on the Strait and did not utilize time variable winds or forcing conditions on either end of the Strait. Thus, here we can analyze this further by looking at the impact of both barotropic and baroclinic bulk pressure gradients and of the winds on the pressure gradients. There is also a statistically significant correlation between the exchange flow and the bulk barotropic pressure gradient ($r = 0.57$, $p = 0$) in the full simulation suggesting that sea surface setup also plays an important role in driving the exchange flow. Using the 8 day filtered principle axes along-coast wind stress (rotation angle = 83.7°, i.e., approximately N/S) (i.e., from Austin and Barth, 2002 adapted as in Giddings et al., 2014), we find statistically significant correlations between the principle axes, along-coast winds (i.e., upwelling versus downwelling) and both the along-Strait bulk baroclinic ($r = 0.52$, $p = 0$) and barotropic ($r = -0.68$, $p = 0$) pressure gradients (see Figure 7a). Importantly, when the winds are downwelling-favorable ($W_{8d} > 0$) the bulk pressure gradients trend towards the opposite of that expected to drive a traditional estuarine exchange flow, i.e., the baroclinic pressure gradient becomes less negative and tends toward 0 and the barotropic pressure gradient becomes $< 0$, increasing in magnitude as the winds increase. A regression analysis of the along-coast winds versus the exchange flow exhibits the strongest correlation ($r = -0.70$, $p = 0$, Figure 7b) explaining nearly 50% of the variance, with strongly downwelling favorable winds ($W_{8d} > 0$) favoring reduced or reversed exchange flow ($Q_{in} < 0$).

Winds along estuarine axes are known to alter exchange flow with winds directed into the estuary reducing exchange and flow out of the estuary enhancing exchange (e.g., Hansen & Rattray, 1965; Scully et al., 2005). A similar analysis to the above but with cross-shore (i.e., nearly along-Strait) winds shows that while there are statistically significant correlations between the along-Strait winds and the bulk pressure gradients (baroclinic $r = -0.52$, $p = 0$; barotropic $r = 0.34$, $p = 0$), the correlations are in the opposite directions as expected and the correlation coefficient of the along-Strait winds with the bulk barotropic pressure gradients is significantly less in magnitude than with the alongshore winds. Interestingly, despite the significant correlation between the along-Strait winds and the bulk pressure gradients, there is not a statistically significant correlation between the along-Strait winds and the exchange flow ($r = 0.17$, $p = 0.063$) suggesting that while the along-Strait winds can impact the bulk pressure gradients (particularly the baroclinic), they are not a dominant driver of the exchange flow.

The approach above uses a bulk baroclinic pressure gradient calculated from the density distributions at the Strait entrance and Race Rocks. Alternatively, we can follow Martin and MacCready (2011) even more closely and calculate the volume averaged incoming momentum terms (meaning the volume average of each subtidal momentum term over just the volume of incoming water). This approach is beneficial in that

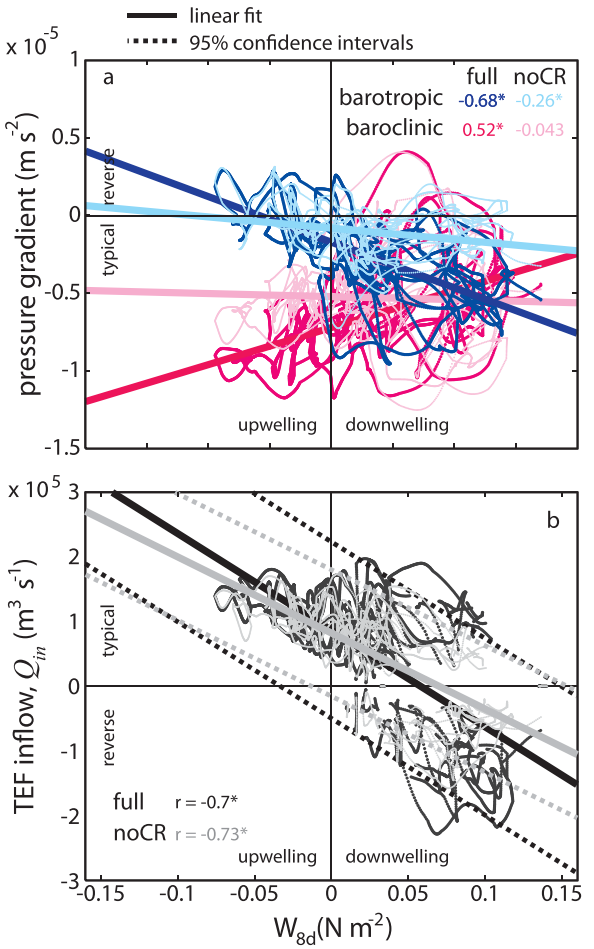


**Figure 7.** Coastal winds versus bulk along-Strait pressure gradients and the Total Exchange Flow. Correlations of the principle axes cumulative 8 day wind stress, $W_{8d}$, similar to that described in Austin and Barth (2002) but employed as a filter to retain the units of stress (see Giddings et al., 2014), where $>0$ is downwelling favorable with (a) the bulk along-Strait pressure gradients (pink = baroclinic, blue = barotropic) and (b) the TEF $Q_{in}$ at section J2C in the center of the Strait. In this case $Q_{in}$ is defined as $-Q_{in}$ when $\Delta S<0$ such that $Q_{in}<0$ indicates reversed exchange flow. For both subplots, darker colors are from the full simulations; lighter colors are from the noCR simulations (the latter is described in section 3.3); and the correlation coefficient values ($r$) are included (where a * indicates the correlation is significantly different from 0 within 95% confidence intervals). Linear best fits (solid lines) with 95% confidence intervals (dashed lines) are included. The latter is excluded from plot (a) for clarity.

it allows for calculation of mean forcing terms over time and across the Strait for all terms. The difficulty is that this analysis does not explicitly account for the direction of the exchange flow, so we enforce that if the exchange flow is reverse ($\Delta S<0$), then the term itself must have a negative sign (as must the exchange flow itself). Using this analysis (plots not shown) results in an even stronger correlation between the pressure gradients and the exchange flow (baroclinic $r=0.98$, $p=0$; barotropic $r=0.55$, $p=0$) but similar correlations between the along-coast winds and these pressure gradients (baroclinic $r=-0.68$, $p=0$; barotropic $r=-0.51$, $p=0$). Equally strong significant (but in the opposite direction) correlations between the incoming volume-averaged Coriolis force and the exchange flow and between the along-coast winds and Coriolis force are found (again indicating the predominant geostrophic balance). Given the predominance of geostrophy and significant topographic effects of the Strait, again an analysis of CAP is beneficial. Here CAP is statistically significantly correlated with the exchange flow ($r=-0.74$, $p=0$) and the along-coast winds ($r=0.46$, $p=0$).

These various analyses indicate that despite the along-stream variations in the momentum balance due to local adjustments, the overall exchange flow is driven predominantly by the pressure gradients (as would be suggested by classical estuarine theories). These pressure gradients are in part established by the direction and strength of the coastal winds, particularly their along-coast direction—upwelling versus downwelling. As geostrophy and other local adjustments (i.e., Coriolis and advection) are also important and act to reduce the contribution of the pressure gradients to the acceleration, the term CAP is a valuable tool to account for these adjustments. CAP is also strongly correlated with the winds and with the exchange flow. Thus while Coriolis, advection, and pressure gradients are all dominant terms in the momentum balance, the response to remote winds can still be thought of as being driven by classical estuarine theories: remote winds alter the baroclinic and barotropic pressure gradients by altering density and sea level at the mouth which are the fundamental drivers of the strength and direction of the exchange flow. Coriolis and advection act to counteract these pressure gradients locally in response to geostrophy and local topography, thus altering the cross-sectional distribution of the exchange flow, and in several along-strait locations reducing the strength of portion of the pressure gradients driving the exchange flow. There are also likely direct impacts of the Coriolis and advection terms at the Strait entrance as the offshore along-coast winds lead to direct advection into (out of) the Strait due to Ekman transport during upwelling (downwelling). The importance of this type of direct Ekman transport was proposed by Holbrook and Halpern (1982). Overall, the along-coast winds offshore of the estuary mouth, over the shelf, account for approximately 50% of the variability in the exchange flow. These results extend the steady analysis of Martin and MacCready (2011) to unsteady conditions. In particular, Martin and MacCready (2011) show that local rectification contributes significantly to the residual while the remainder takes the form of a density driven—viscous exchange. They also highlight the weak effects of friction on the upper layer, also seen here, which allows additional applied forcing (such as that due to the CR plume baroclinic pressure gradient) to dominate the exchange.

#### 3.2.3. Along-Estuary Variability

While there is variability in the lateral patterns of flow and drivers along the Strait, the overall patterns are consistent. On average, incoming flow occurs at high salinity classes (>33 psu) along the entire length of the Strait and outgoing flow occurs at low salinity classes (<33 psu). As one moves into the estuary, the value of $Q_{in}$ decreases

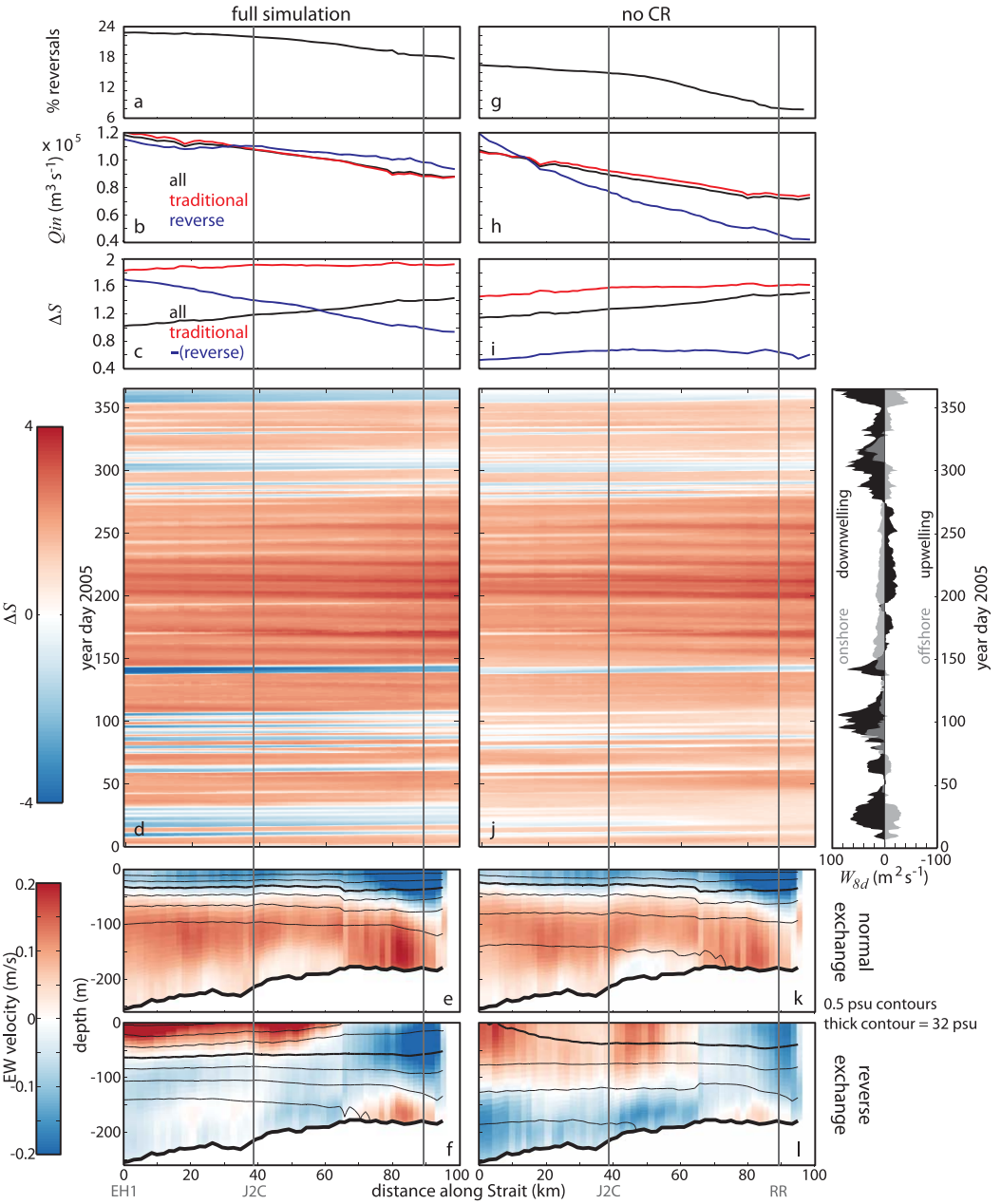


**Figure 8.** Along-Strait TEF variations. (a and g) Percent of time that reversals occur along the Strait in 2005. (b and h) Mean $Q_{in}$ and (c and i) $\Delta S$ along the strait during 2005. In (b, h, c, and i), the entire time series is shown in black, but is also split into traditional exchange directions (red) and reverse exchange (blue). Note that $\Delta S$ during reverse conditions has a negative sign, so the absolute value of $\Delta S$ is shown in blue. (d and j) $\Delta S$ over time and distance along the Strait. Note that here time is the *y* axis and the winds are shown in the far right panel for reference. Along-thalweg mean salinity (contours) and east/west velocity (color) during normal (e and k) and reverse (f and l) exchange conditions. Note that the apparent switch in conditions near km 65 is due to an abrupt change in the bathymetry splitting into a more complex shape where the thalweg is no longer as clearly defined. The left plots (a–f) show results from the full simulation while the right plots (g–l) show results from the noCR simulations (the latter is described below in section 3.3). The locations of the EH1, J2C, and RR sections discussed in the text and shown in other figures are marked with vertical lines and labels along the *x* axis.

approximately linearly (see Figure 8b). Similarly $\Delta S$ increases smoothly along the Straight with the value somewhat higher inland than towards the mouth (Figure 8c). A plot of the time mean east/west flow along the thalweg shows slight variation in the depth of flow reversal (getting deeper moving inland) and shows the slightly outward (third layer) flow at the bottom over part of the estuary (closer to the mouth, Figure 8e).

Examining the time mean momentum terms along the thalweg, the patterns are consistent with that presented in the prior section: the CAP terms dominate the observed acceleration with the baroclinic pressure gradient playing the dominant role, adjusted in magnitude by Coriolis and advection (presented in the following section). Similarly we employed a momentum balance within the TEF framework (i.e., subtidal momentum balance in salinity classes rather than depth bins) and found consistent results along the length of the Strait. At high salinity classes (>33 psu), the baroclinic pressure gradient is largely into the estuary and at lower salinity classes (<33 psu), the baroclinic pressure gradient is largely out of the estuary. The Coriolis term is often opposite that of the baroclinic pressure gradient. This separation in salinity classes matches the incoming (33–34 psu) and outgoing (<33 psu) salinity classes during regular estuarine circulation (e.g., Figure 4). The analysis of CAP in the TEF framework shows it dominates the acceleration, however there is not a clear connection between the acceleration and the exchange flow direction.

Full TEF reversals (as defined by $\Delta S < 0$) occur 23% of the time at the mouth and decrease inland (Figure 8a). This suggests that the drivers of the reversals originate from the ocean end. Note that this is significantly less than 60% of the time that CR water is detected in the Strait and winds are downwelling-favorable. This difference is attributed to other mechanisms which can lead to CR water inside of the Strait including partial reversals, CR mixed with oceanic water offshore, and CR water mixed within the Strait during a previous reversal. During TEF reversals, $Q_{in}$ remains largest at the mouth, but the sign of $\Delta S$ is reversed and its magnitude is greatest at the mouth (Figures 8b and 8c). Contours of $Q_{in}$ (not shown) and $\Delta S$ over the length of the Strait show clear propagation inward from the mouth during regular and reversed exchange events (Figure 8d). During reversals, a cross section of mean salinity and velocity over the length of the Strait in the thalweg (Figure 8f) also clearly shows the inflow coming from the estuary mouth. This signal breaks down around 65 km into the Strait because the bathymetry there is complex with a large sill. While the flow along the thalweg makes it appear that the flow is not reversed this far into the Strait, it does indeed reverse when using the full cross section analysis of TEF.

A lagged correlation of $\Delta S$ (or $Q_{in}$) over the distance of the Strait indicates a lag between the mouth and farther into the estuary consistent with a signal propagation speed of approximately 0.62 m $s^{-1}$ (0.55 m $s^{-1}$) which is considerably faster than the subtidal velocity (about 0.1 m/s) but is close to a typical baroclinic wave speed of 0.53 m $s^{-1}$ (calculated for non-rotating 1$^{st}$ mode with constant $N$ from $\Delta\rho = 2$ kg $m^{-3}$ and depth, $h = 140$ m, using $c_p = Nh/\pi$). During reversals, using actual values of $S_{in}$ and $S_{out}$, and the mean cross-sectional depth (140 m), $c_p$ can be as large as 0.8 m $s^{-1}$ but is typically around 0.5–0.6 m $s^{-1}$. The propagation speed suggests that the baroclinic pressure gradient signal can propagate upstream as a first mode baroclinic wave. This is consistent with an idealized analytical model that used a frictional wave model in the ocean and free-wave equations in the Strait coupled through a Green's function to show that reverse exchange events in the Strait were decently represented by a first mode baroclinic Kelvin wave propagating into the Strait (Proehl & Rattray, 1984). It is important to point out that while this idealized model decently represented reverse exchange conditions, it over-predicted their magnitude and could not represent regular exchange conditions. These shortcomings of the analytical model points to those conditions being maintained by the longer-term along-Strait pressure gradients as in the typical estuarine exchange theory. It is also interesting to note that an analysis of the composite Froude number (using either the TEF variables for a two-layer analysis or a continuous Froude number) approaches or exceeds the critical value of 1 only during reversals (although only occasionally). This suggests that during reversed exchange flow the estuary may occasionally approach hydraulic control, while during normal exchange it behaves more like a classical, viscous estuary (where a balance between the pressure gradient dominated CAP and viscosity drive the residual circulation).

### 3.3. The Influence of the CR Plume

During normal exchange flow conditions, there is minimal influence of the CR plume. This is anticipated as normal exchange flow dominates during upwelling-favorable winds when the CR plume is spread south and offshore, i.e., far away from the Salish Sea. Comparisons of momentum budgets throughout the Strait with and without the CR plume during normal exchange conditions are very similar. If the spin-up cap is chosen to be short enough, some differences begin to emerge as the flow is adjusting from reverse conditions.

During reverse exchange flow conditions, there is a clear and significant impact of the CR plume. Reversal events are much stronger and more surface intensified due to the presence of the CR (see Figures 8f and 8l

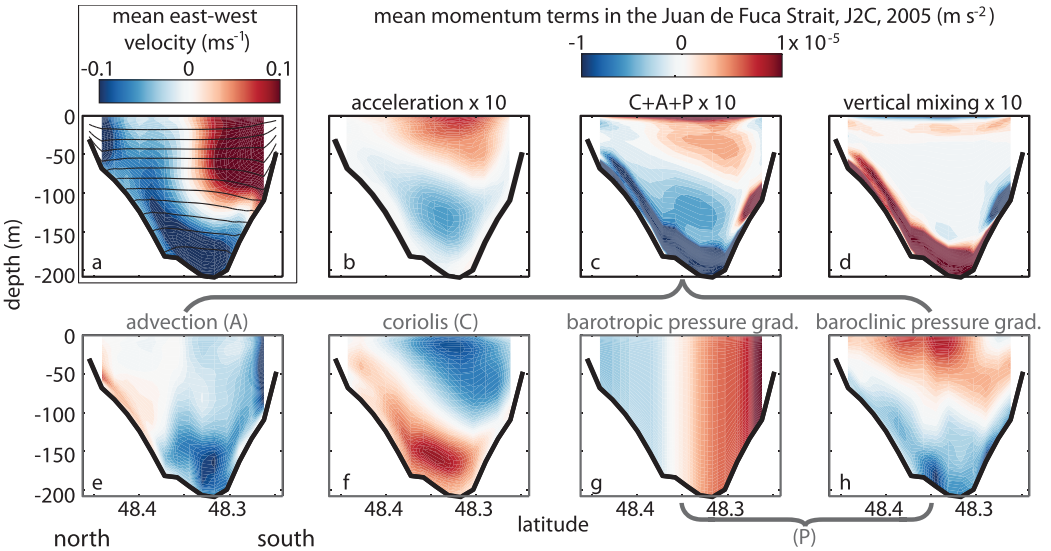


**Figure 9.** Momentum terms in the center of the Strait of Juan de Fuca during exchange reversal spin-up—noCR. Similar to Figure 6 but with the simulations without the presence of the CR.

and also compare Figures 6a and 9a) and they occur significantly more frequently and last longer with the CR plume presence than without (see Figures 8a and 8g). The total time experiencing reverse exchange in 2005 in the full simulations is nearly 40 days (over 21 separate events), while the time is only 25 days (over 18 events) without the CR (noCR simulations).

Without the presence of the CR, the exchange flow still reverses, however the structure switches from a vertically sheared to a more laterally sheared exchange. The inflow is largely constrained to the southern half of the channel, but reaches significantly deeper into the water column and the isohalines no longer have significant slope. The momentum balance terms have a similar structure to the full simulation reversals, however the Coriolis and baroclinic pressure gradient terms take on rather different vertical and lateral structure, and the barotropic pressure gradient now dominates over the baroclinic. The mean baroclinic pressure gradient during reversals decreases by 55% to $2.3 \times 10^{-6}$ without the CR relative to the full simulations. This is counteracted by adjustments in the mean acceleration, advection, and Coriolis terms decreasing by 44%, 23%, and 37%, respectively; whereas the mean barotropic pressure gradient and vertical mixing change by less than 1% between the two simulations. The same trends hold true throughout the Strait as shown in Figure 10. This suggests that the presence of the CR plume directly impacts both the baroclinic pressure gradient and the Coriolis and advection adjustment terms and plays a leading role in the observed exchange flow events.

Without the CR, during reversals the baroclinic density gradient still plays a dominant role (e.g., Figure 10p). However, the baroclinic pressure gradient is weaker and thus the barotropic pressure gradients play a larger relative role balanced by advection and Coriolis (see Figures 9 and 10). This shows that downwelling alone can reverse the exchange, but the baroclinic mechanism is significantly weaker and there is a more dominant role of the sea surface setup and potentially direct Ekman transport. This is seen most clearly in Figure 7 where the noCR simulations are in lighter colors. There is no longer a statistically significant correlation between the winds and the bulk baroclinic pressure gradient without the CR plume offshore (Figure 7a). Additionally, the correlation between the winds and the barotropic pressure gradient is reduced. This may in part be due to more variation in these terms along the Strait and the chosen endpoints to calculate a bulk pressure gradient, as the incoming volume-averaged baroclinic term remains significantly correlated with the along-Strait winds. Nevertheless, in both analyses (bulk versus incoming volume averaged), the correlation between the baroclinic pressure gradient and the exchange flow remains significant. However, while CAP remains significantly correlated with $Q_{in}$ ($r = -0.52$, $p = 0$), it is no longer statistically significantly correlated with the along-coast winds ($r = 0.11$, $p = 0.21$) as it is with the CR present. Importantly, correlation between the winds and the TEF remains high (Figure 7b). Thus, the driving mechanisms are more difficult to tease out without the presence of the CR plume. The baroclinic pressure gradient still plays a role in

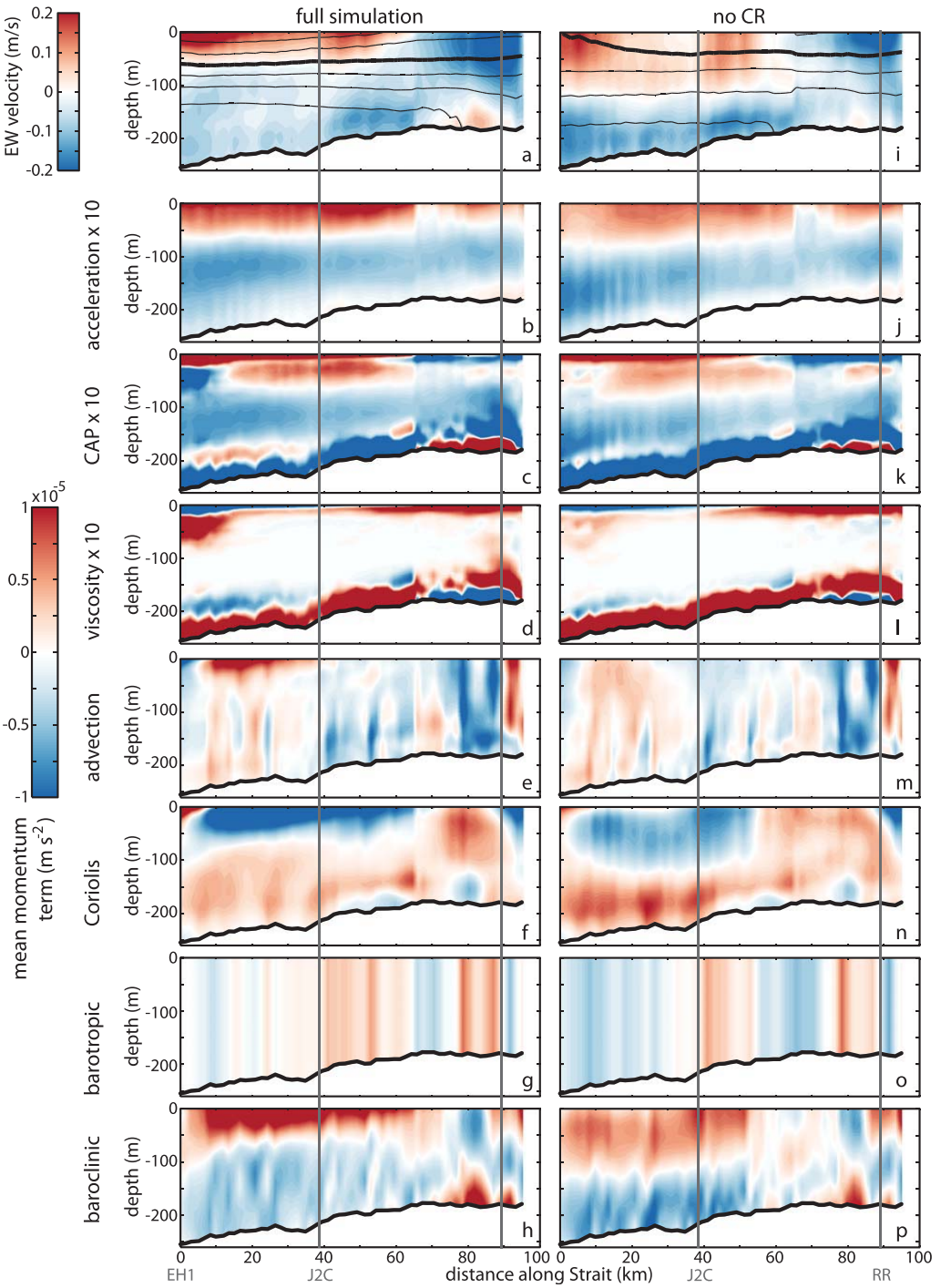


**Figure 10.** Momentum terms along the thalweg of the Strait of Juan de Fuca during exchange reversal spin-up. Similar to Figure 9 but along the thalweg rather than through a cross section. Left plots show the full simulations, right plots show the simulations without the presence of the CR, both show reversed exchange spin-up only ($\Delta S < 0$). Note that as in Figures 5, 6, and 9 the acceleration, CAP, and mixing terms are multiplied by 10 (i.e., they are an order of magnitude smaller than the other terms).

reverse exchange events, but is significantly weaker. The barotropic pressure gradient and local adjustment terms are stronger relative to the baroclinic pressure gradient. These results highlight the strong role that the offshore CR plume has on the exchange flow, but at the same time highlights that the exchange flow is impacted by the offshore winds in a complex manner.

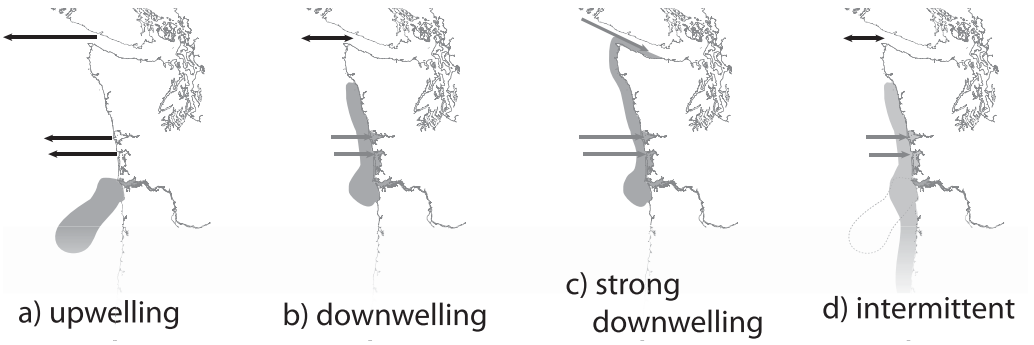


**Figure 11.** Surface estuarine flow in the Northeast Pacific during different wind conditions. The surface flow of the TEF indicated with arrows along the major Washington coastline estuaries. The flow in the Salish Sea and the CR plume (latter in gray) is directly modeled in this paper. The arrows for Grays Harbor and Willapa Bay are deduced from the theory presented here and supported by observations (e.g., Banas et al., 2004; Duxbury, 1979; Hickey & Banas, 2003; Hickey et al., 2002; Roegner et al., 2002). As described in section 1, coastal Oregon estuaries also experience enhanced exchange during upwelling (e.g., Brown & Ozretich, 2009; de Angelis & Gordon, 1985).

## 4. Summary/Conclusions

Along the Northeast Pacific Ocean coast, the estuarine exchange flow is enhanced during the upwelling season relative to the downwelling season. The Columbia River plume strongly interacts with and even intrudes into other estuaries alongshore during downwelling conditions. This increases estuary-estuary connectivity and alters estuary-ocean connectivity. The offshore presence of this river plume also plays an important dynamical role, reducing and sometimes reversing the estuarine exchange flow in the Salish Sea. We anticipate that this response occurs in all of the estuaries north of the CR mouth as corroborated by observations (e.g., Banas et al., 2004; Duxbury, 1979; Hickey and Banas, 2003; Hickey et al., 2002; Roegner et al., 2002). Figure 11 sketches the differences between seasons and their impact on exchange flow and river plumes in the Northeast Pacific region.

The mechanism for these remote forcing impacts is in part described in Figure 12: upwelling enhances traditional along-estuary pressure gradients (both baroclinic and barotropic) thus enhancing exchange flow, while downwelling reduces these gradients leading to reduced, and sometimes reversed exchange flow. The presence of an offshore river plume further reduces/reverses these pressure gradients, particularly the baroclinic pressure gradient, and thus the exchange flow. However, our momentum analysis showed that the processes are a bit more complicated as advection and Coriolis also play an important role adjusting the cross-sectional structure and magnitude of the exchange flow due to local adjustments throughout most of the strait and through direct Ekman transport from the coast into the estuary near the mouth during reversals. Cross-shore (i.e., along-Strait) winds can also impact the pressure gradients, however they are not a dominant driver of the exchange flow. The importance of offshore winds and related upwelling/

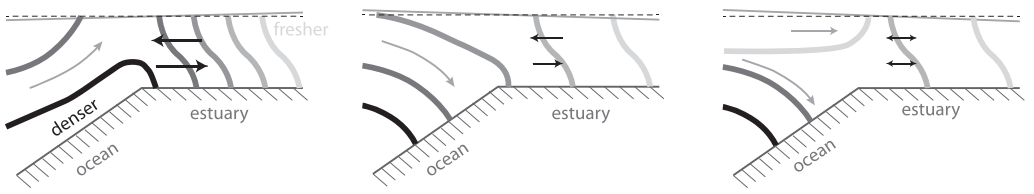


**Figure 12.** Simplified estuarine exchange theory for estuaries along a strong upwelling coast. This sketch (a and b adapted from Hickey et al., 2002, Figure 11) provides an approximate outline of what might be expected for estuaries along upwelling coastlines during different wind conditions. Contours show isopycnals (darker = denser), the dashed line shows a flat sea surface, and black arrows show the direction and strength of the estuarine exchange flow. Impacts may be reduced or enhanced depending upon the type of estuary (well-mixed, strongly stratified, highly seasonal, etc.). This sketch does not include the impacts of Coriolis within the estuary leading to lateral flow variation as observed in the Strait of Juan de Fuca and would be expected in estuaries with a large Rossby radius.

downwelling on estuarine exchange has been previously highlighted in the fjord literature (e.g., Aure et al., 1996; Stigebrandt, 1990), however these systems were well described by two-layer box models, whereas here we highlight a system where a two-layer model does not apply and address the additional complexities adjusting the exchange flow.

We hypothesize that these types of impacts of remote wind forcing (upwelling versus downwelling, and the presence of neighboring along-coast estuaries with significant river plumes) will play an important role for estuaries along upwelling coastlines worldwide. This is in part borne out by observations which have shown enhanced exchange during upwelling conditions in regions all along the North American coastline and the coast of South Africa, and elsewhere (e.g., Gilcoto et al., 2007; Hickey & Banas, 2003; Hickey et al., 2002; Monteiro & Largier, 1999) as well as observations which show intrusions of neighboring/nearby plume water into estuaries during downwelling (e.g., Roegner et al., 2002). We also hypothesize that a major river plume is not necessary to enhance the downwelling impacts, but rather a coastal current formed from multiple smaller river plumes could act as an offshore driver. For example, Mazzini et al. (2014) have shown that coastal Oregon estuaries can combine into a larger scale coastal current impacting a significant portion of the Oregon coastline.

Additionally, while we focus on downwelling and the impact of an offshore plume to the north during downwelling conditions, large adjacent estuaries can also impact neighboring estuaries during upwelling and in particular upwelling to downwelling transitions. For example, Figure 11d shows that during intermittent wind conditions and/or transitions between upwelling and downwelling, the CR plume can reach the Oregon coastline where we might expect it to impact coastal Oregon estuaries with similar mechanisms to those described here. Prior research has shown coastal Oregon estuaries experience enhanced exchange during upwelling (e.g., Brown & Ozretich, 2009; de Angelis & Gordon, 1985) and observations by Mazzini et al. (2015) document the delivery of Columbia River plume water to estuaries south of the Columbia during a wind reversal event. Further analysis during intermittent winds and/or transitions would be an interesting future research direction.

Thus, while this manuscript describes in detail the offshore forcing mechanisms of the economically important Salish Sea and the importance of the neighboring CR, the physics are more generally applicable to a broad array of estuaries. Additionally, these physical mechanisms have broad implications on exchange of nutrients, hypoxic, and acidic waters between estuaries and the coastal ocean, thus dramatically influencing the estuarine ecosystem response (e.g., Davis et al., 2014; Roegner et al., 2011, 2002). These dynamics are critical to understanding estuarine response to climate change that will include altered forcing conditions upstream but also downstream. The impact of downstream forcing changes (including changes in the strength and timing of upwelling and downwelling and the alteration of offshore water masses) on estuarine circulation and ecosystem function can be hypothesized given this improved understanding of estuarine response to remote forcing.

**Acknowledgments**

Thanks to Barbara Hickey, Kristen Davis, Samantha Siedlecki, and Neil Banas for model development and useful scientific discussions. Special thanks to B. Hickey and S. Geier (multiyear moored sensors) from the ECOHAB-PNW and RISE projects, R. Thomson (moored arrays and CTD data, Fisheries and Oceans Canada Institute of Ocean Sciences, IOS), for use of their data. Thanks to other members of the PNWTOX and UWCMG groups for useful discussions including M. Foreman, R. Thomson, I. Fine, E. Lessard, S. Lubetkin, R. McCabe, D. Sutherland, and K. Thyng. D. Darr, and the SIO IT team provided computer cluster administration and support. In addition, we would like to acknowledge high-performance computing support from Yellowstone (ark:/85065/d7wd3xhc) provided by NCAR's Computational and Information Systems Laboratory, sponsored by the National Science Foundation. Access to model run setup files and derived output used in this manuscript are available upon request as described here: iodlabs.ucsd.edu/sgiddings/PNWTOX/contact.html. These model setup files and output data are curated by Giddings on Giddings' server at SIO as well as on MacCready's server at UW and will remain curated for at least 5 years. Initial model development was supported by grants from the Coastal Ocean Program of the National Oceanic and Atmospheric Administration (NOAA) (NA09NOS4780180) and the National Science Foundation (NSF) (OCE0942675) as part of the Pacific Northwest Toxins (PNWTOX) project (SNG and PM). This work was supported by NSF OCE Postdoctoral Research Fellowship 1226406 (SNG) and NSF OCE1634148 (PM). The statements, findings, conclusions, and recommendations are those of the participants/authors and do not reflect the views of NSF, NOAA, or the Department of Commerce.

## References

Armi, L., & Farmer, D. M. (1986). Maximal 2-layer exchange through a contraction with barotropic net flow. *Journal of Fluid Mechanics*, *164*, 27–51. https://doi/org/10.1017/s0022112086002458

Arneborg, L. (2004). Turnover times for the water above sill level in Gullmar Fjord. *Continental Shelf Research*, *24*(4), 443–460.

Arneborg, L., Erlandsson, C. P., Liljebladh, B., & Stigebrandt, A. (2004). The rate of inflow and mixing during deep-water renewal in a sill fjord. *Limnology and Oceanography Methods*, *49*(3), 768–777.

Aure, J., Molvær, J., & Stigebrandt, A. (1996). Observations of inshore water exchange forced by a fluctuating offshore density field. *Marine Pollution Bulletin*, *33*(1), 112–119.

Austin, J. A., & Barth, J. A. (2002). Variation in the position of the upwelling front on the Oregon shelf. *Journal of Geophysical Research*, *107*(C11), 3180. https://doi/org/10.1029/2001JC000858

Babson, A. L., Kawase, M., & MacCready, P. (2006). Seasonal and interannual variability in the circulation of Puget Sound, Washington: A box model study. *Atmosphere-Ocean*, *44*(1), 29–45. https://doi/org/10.3137/ao.440103

Banas, N. S., Hickey, B. M., MacCready, P., & Newton, J. A. (2004). Dynamics of Willapa Bay, Washington: A highly unsteady, partially mixed estuary. *Journal of Physical Oceanography*, *34*(11), 2413–2427.

Banas, N. S., MacCready, P., & Hickey, B. M. (2009a). The Columbia River plume as cross-shelf exporter and along-coast barrier, *Physics of Estuaries and Coastal Seas: Papers From the PECS 2006 Conference*, *29*(1), 292–301. https://doi/org/10.1016/j.csr.2008.03.011

Banas, N. S., McDonald, P., & Armstrong, D. (2009b). Green crab larval retention in Willapa Bay, Washington: An intensive Lagrangian modeling approach. *Estuaries and Coasts*, *32*(5), 893–905. https://doi/org/10.1007/s12237-009-9175-7

Battisti, D. S., & Hickey, B. M. (1984). Application of remote wind-forced coastal trapped wave theory to the Oregon and Washington coasts. *Journal of Physical Oceanography*, *14*(5), 887–903. https://doi/org/10.1175/1520-0485(1984)0142.0.CO;2

Bowen, M. M., & Geyer, W. R. (2003). Salt transport and the time-dependent salt balance of a partially stratified estuary. *Journal of Geophysical Research*, *108*(C5), 3158. https://doi/org/10.1029/2001JC001231

Boyer, E. W., Goodale, C. L., Jaworski, N. A., & Howarth, R. W. (2002). Anthropogenic nitrogen sources and relationships to riverine nitrogen export in the northeastern U.S.A. *Biogeochemistry*, *57–58*(1), 137–169. https://doi/org/10.1023/A:1015709302073

Brown, C., & Ozretich, R. (2009). Coupling between the Coastal Ocean and Yaquina Bay, Oregon: Importance of oceanic inputs relative to other nitrogen sources. *Estuaries and Coasts*, *32*(2), 219–237. https://doi/org/10.1007/s12237-008-9128-6

Cannon, G. A. (1978). *Circulation in the Strait of Juan de Fuca: Some recent oceanographic observations* (NOAA Tech. Rep. ERL 399-PMEL 29). Seattle, WA: National Oceanic and Atmospheric Administration.

Chatwin, P. C. (1976). Some remarks on the maintenance of the salinity distribution in estuaries. *Estuarine and Coastal Marine Science*, *4*(5), 555–566.

Chen, S.-N., Geyer, W. R., Ralston, D. K., & Lerczak, J. A. (2012). Estuarine exchange flow quantified with isohaline coordinates: Contrasting long and short estuaries. *Journal of Physical Oceanography*, *42*(5), 748–763. https://doi/org/10.1175/JPO-D-11-086.1

Cloern, J. E., Jassby, A. D., Thompson, J. K., & Hieb, K. A. (2007). A cold phase of the East Pacific triggers new phytoplankton blooms in San Francisco Bay. *Proceedings of the National Academy of Sciences of the United States of America*, *104*(47), 18561–18656.

Computational and Information Systems Laboratory (2012). *Yellowstone: IBM iDataPlex System* (University Community Computing). Boulder, CO: National Center for Atmospheric Research. Retrieved from http://n2t.net/ark:/85065/d7wd3xhc

Connolly, T. P., Hickey, B. M., Shulman, I., & Thomson, R. E. (2014). Coastal trapped waves, alongshore pressure gradients, and the California undercurrent. *Journal of Physical Oceanography*, *44*, 319–342. https://doi/org/10.1175/JPO-D-13-095.1

Davis, K. A., Banas, N. S., Giddings, S. N., Siedlecki, S. A., MacCready, P., Lessard, E. J., . . . Hickey, B. M. (2014). Estuary-enhanced upwelling of marine nutrients fuels coastal productivity in the U.S. Pacific Northwest. *Journal of Geophysical Research: Oceans*, *119*, 8778–8799. https://doi/org/10.1002/2014JC010248

de Angelis, M. A., & Gordon, L. I. (1985). Upwelling and river runoff as sources of dissolved nitrous oxide to the Alsea estuary, Oregon. *Estuarine Coastal and Shelf Science*, *20*(4), 375–386. https://doi/org/10.1016/0272-7714(85)90082-4

Duxbury, A. C. (1979). Upwelling and estuary flushing. *Limnology and Oceanography*, *24*(4), 627–933.

Emery, W. J., & Thomson, R. E. (2004). *Data analysis methods in physical oceanography* (638 pp.). Amsterdam, the Netherlands: Elsevier.

Fong, D. A., & Geyer, W. R. (2001). Response of a river plume during an upwelling favorable wind event. *Journal of Geophysical Research*, *106*(C1), 1067–1084. https://doi/org/10.1029/2000JC900134

Fong, D. A., & Geyer, W. R. (2002). The alongshore transport of freshwater in a surface-trapped river Plume. *Journal of Physical Oceanography*, *32*(3), 957–972. https://doi/org/10.1175/1520-0485(2002)0322.0.CO;2

Foreman, M. G. G., Smith, C. L., & Chandler, P. (2000). Current simulations and biological transport for the western continental margin of Vancouver Island. In L. R. Bentley, et al., (Eds.), *Computational methods in Water Resources* (Vol. 2, pp. 857–864). Rotterdam: A. A. Balkema.

Frisch, A. S., Holbrook, J., & Ages, A. B. (1981). Observations of a summertime reversal in circulation in the Strait of Juan-De-Fuca. *Journal of Geophysical Research*, *86*(C3), 2044–2048. https://doi/org/10.1029/JC086iC03p02044

Geyer, W. R., & MacCready, P. (2014). The estuarine circulation. *Annual Review of Fluid Mechanics*, *46*(1), 175–197. https://doi/org/10.1146/annurev-fluid-010313-141302

Geyer, W. R., & Ralston, D. K. (2011). The dynamics of strongly stratified estuaries. In E. Wolanski & D. McLusky (Eds.), *Treatise on estuarine and coastal science* (pp. 37–52). Amsterdam, the Netherlands: Elsevier.

Giddings, S. N., MacCready, P., Hickey, B. M., Banas, N. S., Davis, K. A., Siedlecki, S. A., . . . Connolly, T. P. (2014). Hindcasts of potential harmful algal bloom transport pathways on the Pacific Northwest coast. *Journal of Geophysical Research: Oceans*, *119*(4), 2439–2461. https://doi/org/10.1002/2013JC009622

Gilcoto, M., Pardo, P. C., Álvarez-Salgado, X. A., & Pérez, F. F. (2007). Exchange fluxes between the Rìa de Vigo and the shelf: A bidirectional flow forced by remote wind. *Journal of Geophysical Research*, *112*, C06001. https://doi/org/10.1029/2005JC003140

Godin, G., Candela, J., & de la Paz-Vela, R. (1981). An analysis and interpretation of the current data collected in the strait of Juan de Fuca in 1973. *Marine Geodesy*, *5*(3), 273–302. https://doi/org/10.1080/15210608109379424

Griffin, D. A., & Leblond, P. H. (1990). Estuary ocean exchange controlled by spring-neap tidal mixing. *Estuarine Coastal and Shelf Science*, *30*(3), 275–297. https://doi/org/10.1016/0272-7714(90)90052-S

Gustafsson, B. G. (2000). Time-dependent modeling of the Baltic entrance area. 1. Quantification of circulation and residence times in the Kattegat and the straits of the Baltic sill. *Estuaries and Coasts*, *23*(2), 231–252.

Hansen, D. V., & Rattray, M. Jr (1965). Gravitational circulation in straits and estuaries. *Journal of Marine Research*, *23*(2), 104–122.

Herlinveaux, R. H., & Tully, J. P. (1961). Some oceanographic features of Juan De Fuca Strait. *Journal of the Fisheries Research Board of Canada*, *18*(6), 1027–1071.

Hetland, R. D. (2010). Estuarine overmixing. *Journal of Physical Oceanography*, *40*(1), 199–211.

Hickey, B. M. (1979). The California current system—Hypotheses and facts. *Progress in Oceanography*, *8*(4), 191–279. https://doi/org/10.1016/0079-6611(79)90002-8

Hickey, B. M. (1989). Patterns and processes of shelf and slope circulation. In M. R. Landry & B. M. Hickey (Eds.), *Coastal oceanography of Washington and Oregon* (pp. 41–115). Amsterdam, the Netherlands: Elsevier.

Hickey, B. M., & Banas, N. S. (2003). Oceanography of the US Pacific Northwest Coastal Ocean and estuaries with application to coastal ecology. *Estuaries*, *26*(4B), 1010–1031.

Hickey, B. M., Geier, S., Kachel, N., & MacFadyen, A. (2005). A bi-directional river plume: The Columbia in summer. *Continental Shelf Research*, *25*(14), 1631–1656. https://doi/org/10.1016/j.csr.2005.04.010

Hickey, B. M., McCabe, R., Geier, S., Dever, E., & Kachel, N. (2009). Three interacting freshwater plumes in the northern California Current System. *Journal of Geophysical Research*, *114*, C00B03. https://doi/org/10.1029/2008JC004907

Hickey, B. M., Thomson, R. E., Yih, H., & LeBlond, P. H. (1991). Velocity and temperature fluctuations in a buoyancy-driven current off Vancouver Island. *Journal of Geophysical Research*, *96*(C6), 10538–10538. https://doi/org/10.1029/90JC02578

Hickey, B. M., Zhang, X., & Banas, N. (2002). Coupling between the California Current System and a coastal plain estuary in low riverflow conditions. *Journal of Geophysical Research*, *107*(C10), 3166. https://doi/org/10.1029/1999JC000160

Holbrook, J. R., & Halpern, D. (1982). Winter-time near-surface currents in the strait of Juan de Fuca. *Atmosphere-Ocean*, *20*(4), 327–339. https://doi/org/10.1080/07055900.1982.9649149

Holbrook, J. R., Meunch, R. D., Kachel, D. G., & Wright, C. (1980). *Circulation in the Strait of Juan de Fuca: Recent Oceanographic Observations in the Eastern Basin* (NOAA Tech. Rep. ERL 412-PMEL 33). Seattle, WA: National Oceanic and Atmospheric Administration.

Horner-Devine, A. R., Hetland, R. D., & MacDonald, D. G. (2015). Mixing and transport in coastal river Plumes. *Annual Review of Fluid Mechanics*, *47*, 569–594. https://doi/org/10.1146/annurev-fluid-010313-141408

Jackson, R. H., Straneo, F., & Sutherland, D. A. (2014). Externally forced fluctuations in ocean temperature at Greenland glaciers in non-summer months. *Nature Geoscience*, *7*(7), 503–508. https://doi/org/10.1038/ngeo2186

Jay, D. A., & Musiak, J. D. (1996). Internal tidal asymmetry in channel flows: Origins and consequences. In C. B. Pattiaratchi (Ed.), *Mixing processes in estuaries and coastal seas, an American Geophysical Union coastal and estuarine sciences monograph* (pp. 219–258). Washington, DC: American Geophysical Union.

Jay, D. A., & Smith, J. D. (1990). Residual circulation in shallow estuaries 2. Weakly stratified and partially mixed, narrow estuaries. *Journal of Geophysical Research*, *95*(C1), 733–748.

Klinck, J. M., O'brien, J. J., & Svendsen, H. (1981). A simple model of fjord and coastal circulation interaction. *Journal of Physical Oceanography*, *11*(12), 1612–1626.

Knudsen, M. (1900). Ein hydrographischer lehrsatz. *Annalen Der Hydrographie Und Maritimen Meteorologie*, *28*(7), 316–320.

Kosro, P. M., Peterson, W. T., Hickey, B. M., Shearman, R. K., & Pierce, S. D. (2006). Physical versus biological spring transition: 2005. *Geophysical Research Letters*, *33*, L22S03. https://doi/org/10.1029/2006GL027072

Kranenburg, C. (1986). A time scale for long-term salt intrusion in well-mixed estuaries. *Journal of Physical Oceanography*, *16*(7), 1329–1331.

Labrecque, A. J. M., Thomson, R. E., Stacey, M. W., & Buckley, J. R. (1994). Residual currents in juan de Fuca strait. *Atmosphere-Ocean*, *32*(2), 375–394. https://doi/org/10.1080/07055900.1994.9649503

Li, C., White, J. R., Chen, C., Lin, H., Weeks, E., Galvan, K., & Bargu, S. (2011). Summertime tidal flushing of Barataria Bay: Transports of water and suspended sediments. *Journal of Geophysical Research*, *116*, C04009. https://doi/org/10.1029/2010JC006566

Liu, Y., MacCready, P., & Hickey, B. M. (2009a). Columbia River plume patterns in summer 2004 as revealed by a hindcast coastal ocean circulation model. *Geophysical Research Letters*, *36*, L02601. https://doi/org/1 0.1029/2008GL036447

Liu, Y., MacCready, P., Hickey, B. M., Dever, E. P., Kosro, P. M., & Banas, N. S. (2009b). Evaluation of a coastal ocean circulation model for the Columbia River plume in summer 2004. *Journal of Geophysical Research*, *114*, C00B04. https://doi/org/10.1029/2008JC004929

MacCready, P. (2007). Estuarine adjustment. *Journal of Physical Oceanography*, *37*, 2133–2145. https://doi/org/10.1175/JPO3082.1

MacCready, P. (2011). Calculating estuarine exchange flow using isohaline coordinates. *Journal of Physical Oceanography*, *41*(6), 1116–1124. https://doi/org/10.1175/2011JPO4517.1

MacCready, P., Banas, N. S., Hickey, B. M., Dever, E. P., & Liu, Y. (2009). A model study of tide- and wind-induced mixing in the Columbia River Estuary and plume. *Physics of Estuaries and Coastal Seas: Papers from the PECS 2006 Conference*, *29*(1), 278–291. https://doi/org/10.1016/j.csr.2008.03.015

MacCready, P., & Geyer, W. R. (2010). Advances in estuarine physics. *Annual Review of Marine Science*, *2*(1), 35–58. https://doi/org/10.1146/annurev-marine-120308-081015

Martin, W. D., & MacCready, P. (2011). Influence of large-scale tidal asymmetry on subtidal dynamics in the western Strait of Juan de Fuca. *Journal of Geophysical Research*, *116*, C02009. https://doi/org/10.1029/2010JC006363

Masson, D., & Cummins, P. F. (2000). Fortnightly modulation of the estuarine circulation in Juan de Fuca Strait. *Journal of Marine Research*, *58*(3), 439–463.

Mazzini, P. L. F., Barth, J. A., Shearman, R. K., & Erofeev, A. (2014). Buoyancy-driven coastal currents off Oregon during fall and winter. *Journal of Physical Oceanography*, *44*(11), 2854–2876. https://doi/org/10.1175/Jpo-D-14-0012.1

Mazzini, P. L., Risien, C. M., Barth, J. A., Pierce, S. D., Erofeev, A., Dever, E. P., . . . Vardaro, M. F. (2015). Anomalous near-surface low-salinity pulses off the central Oregon coast. *Scientific Reports*, *5*. 17145. https://doi/org/10.1038/srep17145

McConnaughey, R. A., Armstrong, D. A., Hickey, B. M., & Gunderson, D. R. (1994). Interannual variability in coastal Washington Dungeness crab (Cancer magister) populations: Larval advection and the coastal landing strip. *Fisheries Oceanography*, *3*(1), 22–38. https://doi/org/10.1111/j.1365-2419.1994.tb00045.x

McLusky, D. S., & Elliott, M. (2004). *The Estuarine Ecosystem: Ecology, threats, and management* (214 pp.). New York, NY: Oxford University Press.

Monteiro, P. M. S., & Largier, J. L. (1999). Thermal stratification in Saldanha Bay (South Africa) and subtidal, density-driven exchange with the coastal waters of the Benguela upwelling system. *Estuarine, Coastal and Shelf Science*, *49*(6), 877–890. https://doi/org/10.1006/ecss.1999.0550

Moore, S. K., Mantua, N. J., Kellogg, J. P., & Newton, J. A. (2008). Local and large-scale climate forcing of Puget Sound oceanographic properties on seasonal to interdecadal timescales. *Limnology and Oceanography Methods*, *53*(5), 1746–1758. https://doi/org/10.4319/lo.2008.53.5.1746

Newton, J. A., & Horner, R. (2003). Use of phytoplankton species indicators to track the origin of phytoplankton blooms in Willapa Bay, Washington. *Estuaries and Coasts*, *26*(4), 1071–1078. https://doi/org/10.1007/BF02803364

Newton, J. A., Siegel, E., & Albertson, S. L. (2003). Oceanographic changes in Puget sound and the Strait of Juan de Fuca during the 2000–01 Drought. *Canadian Water Resources Journal*, *28*(4), 715–728. https://doi/org/10.4296/cwrj2804715

O'Callaghan, J., Pattiaratchi, C., & Hamilton, D. (2007). The response of circulation and salinity in a micro-tidal estuary to sub-tidal oscillations in coastal sea surface elevation, *Continental Shelf Research*, *27*(14), 1947–1965. https://doi/org/10.1016/j.csr.2007.04.004

Pendleton, L. H. (2008). *The economic and market value of coasts and estuaries: What's at stake? Executive summary*, Arlington, VA: Restore America's Estuaries.

Pritchard, D. W. (1954). A study of the salt balance in a coastal plain estuary. *Journal of Marine Research*, *13*(1), 133–144.

Pritchard, D. W. (1956). The dynamics structure of a coastal plain estuary. *Journal of Marine Research*, *15*(1), 33–42.

Proehl, J. A., & Rattray, M. R., Jr. (1984). Low-frequency response of wide deep estuaries to non-loca1 atmospheric forcing. *Journal of Physical Oceanography*, *14*(5), 904–921. https://doi/org/10.1175/1520-0485(1984)014<0904:LFROWD>2.0.CO;2

Roegner, G. C., Hickey, B. M., Newton, J. A., Shanks, A. L., & Armstrong, D. A. (2002). Wind-induced plume and bloom intrusions into Willapa Bay, Washington. *Limnology and Oceanography*, *47*(4), 1033–1042.

Roegner, G. C., Seaton, C., & Baptista, A. (2011). Climatic and tidal forcing of hydrography and chlorophyll concentrations in the Columbia river estuary. *Estuaries and Coasts*, *34*(2), 281–296. https://doi/org/10.1007/s12237-010-9340-z

Scully, M. E. (2010). Wind modulation of dissolved oxygen in Chesapeake Bay. *Estuaries and Coasts*, *33*(5), 1164–1175. https://doi/org/10.1007/s12237-010-9319-9

Scully, M. E., & Friedrichs, C. T. (2007). The importance of tidal and lateral asymmetries in stratification to residual circulation in partially mixed estuaries. *Journal of Physical Oceanography*, *37*(6), 1496–1511.

Scully, M. E., Friedrichs, C., & Brubaker, J. (2005). Control of estuarine stratification and mixing by wind-induced straining of the estuarine density field. *Estuaries*, *28*(3), 321–326. https://doi/org/10.1007/bf02693915

Shchepetkin, A. F., & McWilliams, J. C. (2005). The regional oceanic modeling system (ROMS): A split-explicit, free-surface, topography-following-coordinate oceanic model. *Ocean Modelling*, *9*(4), 347–404. https://doi/org/10.1016/j.ocemod.2004.08.002

Siedlecki, S. A., Banas, N. S., Davis, K. A., Giddings, S., Hickey, B. M., MacCready, P., . . . Geier, S. (2015). Seasonal and interannual oxygen variability on the Washington and Oregon continental shelves. *Journal of Geophysical Research: Oceans*, *120*, 608–633. https://doi/org/10.1002/2014JC010254

Stacey, M. T., Burau, J. R., & Monismith, S. G. (2001). Creation of residual flows in a partially stratified estuary. *Journal of Geophysical Research*, *106*(C8), 17013–17037.

Stigebrandt, A. (1990). On the response of the horizontal mean vertical density distribution in a fjord to low-frequency density fluctuations in the coastal water. *Tellus, Series A*, *42*(5), 605–614.

Stommel, H., & Farmer, H. G. (1953). Control of salinity in an estuary by a transition. *Journal of Marine Research*, *12*, 12–20.

Straneo, F., & Cenedese, C. (2015). The dynamics of Greenland's glacial fjords and their role in climate. *Annual Review of Materials Science*, *7*, 89–112. https://doi/org/10.1146/annurev-marine-010213-135133

Sutherland, D. A., MacCready, P., Banas, N. S., & Smedstad, L. F. (2011). A model study of the Salish Sea estuarine circulation. *Journal of Physical Oceanography*, *41*(6), 1125–1143. https://doi/org/10.1175/2011JPO4540.1

Sutherland, D. A., Straneo, F., & Pickart, R. S. (2014). Characteristics and dynamics of two major Greenland glacial fjords. *Journal of Geophysical Research: Oceans*, *119*, 3767–3791. https://doi/org/10.1002/2013JC009786

Thomson, R. E., & Krassovski, M. V. (2010). Poleward reach of the California undercurrent extension. *Journal of Geophysical Research*, *115*, C09027. https://doi/org/10.1029/2010JC006280

Thomson, R. E., Mih·Ly, S. F., & Kulikov, E. A. (2007). Estuarine versus transient flow regimes in Juan de Fuca Strait. *Journal of Geophysical Research*, *112*, C09022. https://doi/org/10.1029/2006JC003925

Valle-Levinson, A. (1995). Observations of barotropic and baroclinic exchanges in the lower Chesapeake Bay. *Nearshore and Coastal Oceanography*, *15*(13), 1631–1647. https://doi/org/10.1016/0278-4343(95)00011-O

Valle-Levinson, A. (2011). Large estuaries (effects of rotation). In E. Wolanski & D. S. McLusky (Eds.), *Treatise on estuarine and coastal science* (Vol. 2, pp. 123–140). Waltham, MA: Academic Press.

Valle-Levinson, A., Li, C., Wong, K.-C., & Lwiza, K. M. M. (2000). Convergence of lateral flow along a coastal plain estuary. *Journal of Geophysical Research*, *105*(C7), 17045–17061. https://doi/org/10.1029/2000JC900025

Wang, D. P., & Elliot, A. J. (1978). Non-tidal variability in the Chesapeake Bay and Potomac River: Evidence for non-local forcing. *Journal of Physical Oceanography*, *8*(2), 225–232.

Willmott, C. J. (1982). Some comments on the evaluation of model performance. *Bulletin of the American Meteorological Society*, *63*(11), 1309–1313. https://doi/org/10.1175/1520-0477(1982)0632.0.CO;2

Wong, K.-C., & Lu, X. (1994). Low-frequency variability in Delaware's inland bays, *Journal of Geophysical Research*, *99*(C6), 12683–12695. https://doi/org/10.1029/94JC00569

Yamada, S., & Kosro, P. (2010). Linking ocean conditions to year class strength of the invasive European green crab, *Carcinus maenas*. *Biological Invasions*, *12*(6), 1791–1804. https://doi/org/10.1007/s10530-009-9589-y